Considerations for CO_2 storage in deep saline aquifers in tectonically active regions with implications for the Lower Mainland British Columbia (LMBC)

Maziyar Nazemi[1, *], Shahin E. Dashtgard[1], Hassan Hassanzadeh[2], and Andrew D. La Croix[3]

[1]Applied Research in Ichnology and Sedimentology (ARISE) Group, Department of Earth Sciences, Simon Fraser University, Burnaby, British Columbia, Canada V5A 1S6

[2]Department of Chemical & Petroleum Engineering, Schulich School of Engineering, University of Calgary, 2500 University Drive NW, Calgary, Alberta, T2N 1N4 Canada

[3]Sedimentary Environments and Analogues Research Group, Earth and Environmental Science, Te Aka Mātuatua - School of Science, University of Waikato, Hamilton 3240, New Zealand

*Corresponding author email: *maziyar_nazemi@sfu.ca*

Keywords: CO_2 sequestration; Saline aquifers; Lower Mainland British Columbia; Georgia Basin; *in-situ/ex-situ* CO_2 dissolution

***This paper is a non-peer-reviewed preprint submitted to EarthArXiv.**

***This preprint was initially submitted to the Bulletin of Canadian Energy Geoscience but was later withdrawn by the authors. It will now be submitted to the International Journal of Greenhouse Gas Control.**

Abstract

Underground geological storage of carbon dioxide (CO_2) has emerged as one of the most viable solutions for mitigating global carbon emissions during the transition to a net-zero economy. Within subsurface geological strata, saline aquifers and depleted oil and gas reservoirs are the primary targets for CO_2 storage. However, in regions with limited oil and gas production operations, underground storage is generally assumed to be non-viable or uneconomic even where potential storage capacity is present, and this assumption is further amplified in tectonically active regions. Herein, we review the characteristics of deep saline aquifers necessary for CO_2 storage in tectonically active regions focusing on the Lower Mainland of British Columbia (LMBC), Canada. We discuss the subsurface and reservoir characteristics necessary for successful CO_2 storage and summarize available information from the LMBC.

In the LMBC, conditions for underground storage of CO_2 are favorable in some Tertiary strata below ~1,000–1,264 m depth, especially if *in-situ* or *ex-situ* CO_2 dissolution is employed. Sandstone beds in Tertiary strata between 1,000 and 2,000 m have reservoir characteristics that are favorable for CO_2-brine solution injection, including: permeability (0.1–2,390 mD), porosity (12–23% based on well logs and using a 9% cutoff; 2.4–22.3% measured in core samples), and salinity (751–37,438 ppm), and some sandstone beds show reasonable reservoir capacity (based on drill stem test results). Coal seams in Tertiary strata also have CO_2 storage potential but require further study to quantify their potential. There are large regions of the LMBC where Tertiary strata are situated greater than 5 km and 10 km from mapped faults, and this lowers the potential risk of CO_2-brine leakage.

There is limited data available for Upper Cretaceous strata below the LMBC, and hence, there is greater uncertainty in determining CO_2 storage potential in these strata. Well-log-based porosity ranges from 12.5–20% (using a 9% porosity cutoff), which is favorable for CO_2 storage. Available 2D seismic data shows that Upper Cretaceous rocks below the LMBC are heavily faulted, although many faults terminate at the top of the Upper Cretaceous interval. The distribution of faults increases the potential risk of CO_2 leakage, although the confinement of faults to the Upper Cretaceous suggests the risk of leakage to surface or into shallow aquifers is minimal; this is especially true if *in-situ* or *ex-situ* CO_2 dissolution is employed.

1. Introduction

Increasing carbon dioxide (CO_2) concentrations significantly impact Earth's atmosphere by intensifying the greenhouse effect and warming the planet (Bachu, 2003). Warming is predicted to cause more frequent and intense extreme weather events such as heatwaves, tropical cyclones, heavy precipitation, and flooding

(Flannigan and Wagner, 1991), and extreme weather events increasingly threaten critical infrastructure and society (Bratu et al., 2022). In an effort to minimize anthropogenic warming and associated weather events, a carbon-neutral economy is being pursued (net zero carbon emissions; EIA, 2021). The transition to a carbon-neutral global economy is expected to take decades, meaning that surplus CO_2 emissions will continue for the foreseeable future (Fig. 1; U.S. Energy Information Administration, 2022; Friedlingstein et al., 2022; Friedlingstein et al., 2020). Controlling and reducing atmospheric CO_2 while simultaneously sustaining our standard of living and expanding the standard of living of developing countries require cost-effective and innovative solutions.

Carbon capture and underground storage (CCS) is considered the most viable approach for mitigating CO_2 emissions over the short to medium term (Pachauri et al., 2014). While various carbon storage methods continue to be developed (e.g., ocean storage, mineral carbonation; Ang et al., 2022), CO_2 sequestration in sedimentary basins (geological storage) remains the most economically viable approach (Cao et al., 2020). In this study, we review the critical factors that must be considered in identifying sites for CO_2 sequestration in saline aquifers in tectonically active regions. These factors include geothermal gradient and pressure, reservoir depth and thickness, porewater salinity, mineralogy, porosity-permeability, reservoir pressure and confinement, seismicity, and faults. We summarize available information for these factors for sedimentary strata below the Lower Mainland of British Columbia, Canada (LMBC; Fig. 2) which form part of the Georgia Basin. We then comment on the risks associated with CCS in the LMBC and identify knowledge gaps that must be addressed before CCS feasibility can be assessed fully.

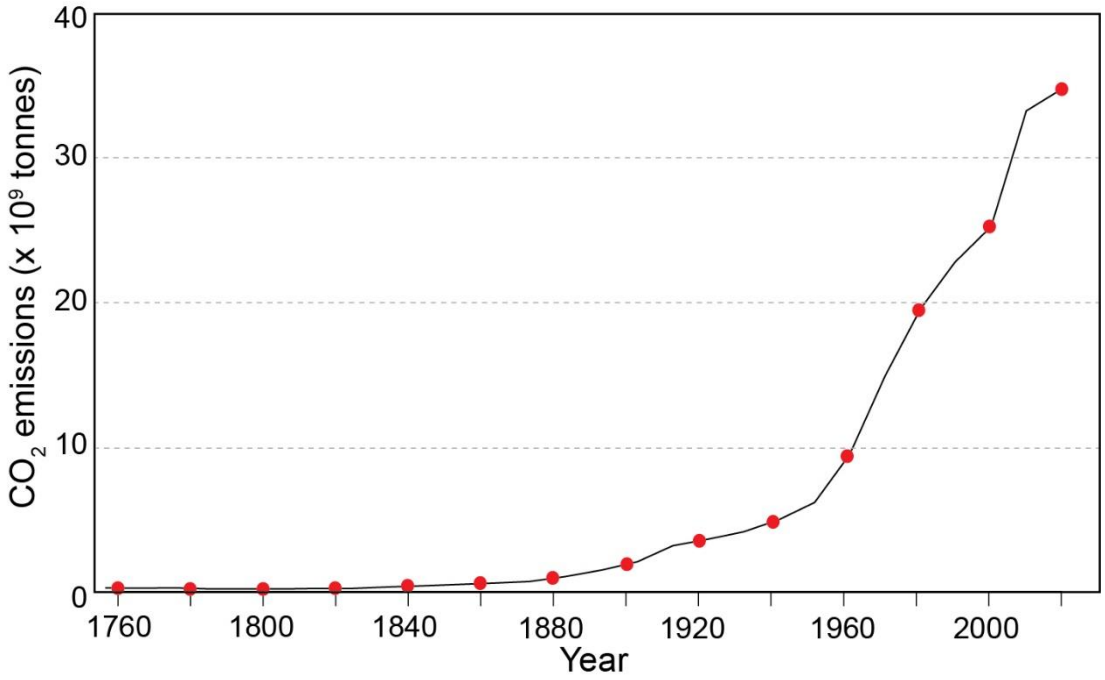

Figure 1 (one column) – CO_2 emissions from global fossil fuel combustion and industrial processes between 1760 and 2020 (modified after Friedlingstein et al., 2020).

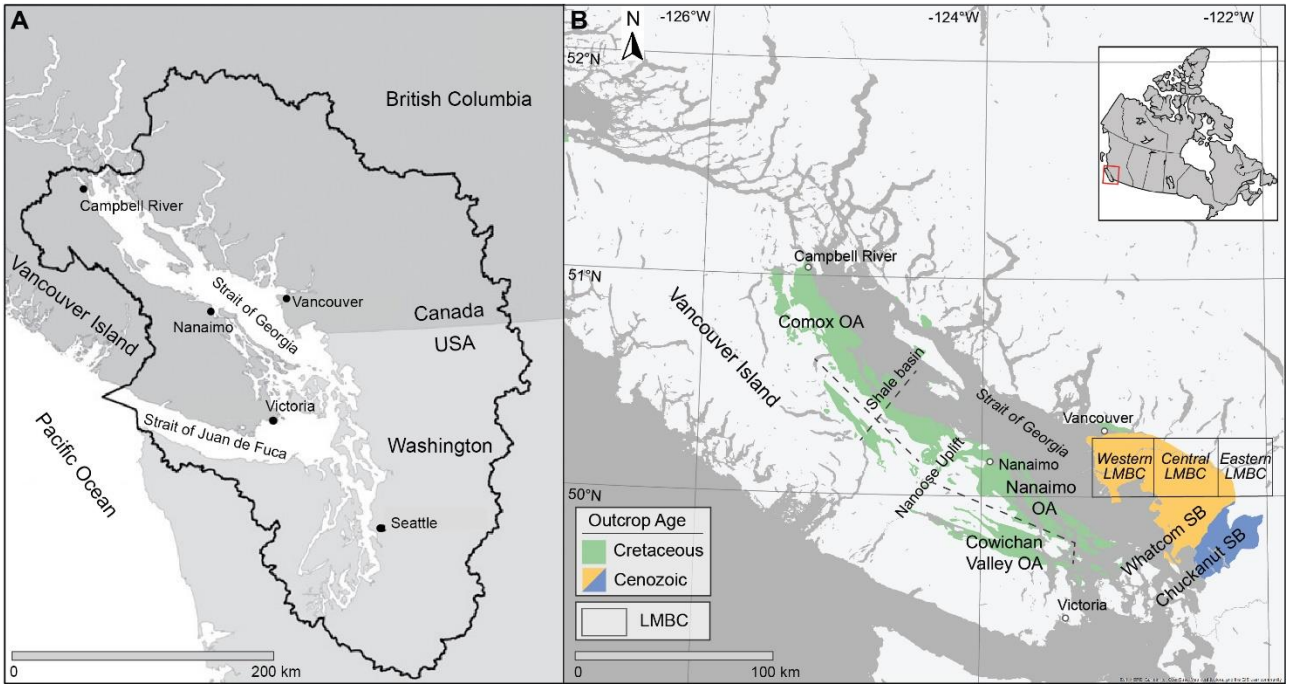

Figure 2 (two columns) – A) The extent of the drainage area (excluding the Fraser River) that comprises the modern Georgia Basin in Canada and the USA (Butler et al., 2019). B) Simplified geological map of pre-Pleistocene sedimentary strata in the Georgia Basin and the location of the study area (LMBC). The inset map shows the position of the Georgia Basin in Canada. Colored polygons show the extent of Upper Cretaceous Nanaimo Group strata exposed in the Comox, Nanaimo, and Cowichan Valley outcrop areas (OA; green); Tertiary strata in the Whatcom

Sub-Basin (SB; orange); and, Tertiary strata in Chukanut SB (blue; modified after Huang et al., 2022). The Western LMBC, Central LMBC, and Eastern LMBC are referred to in the text.

1.2 *Background*

Carbon dioxide is a natural constituent of Earth's atmosphere; however, the significant increase in atmospheric CO_2 concentration since the 19th century (Fig. 1) is largely attributed to human activity and primarily to the combustion of fossil fuels, including coal, oil, and natural gas (CH_4; Keighley and Maher, 2015). In February 2022, the global concentration of CO_2 was 419.3 ppm (Ang et al., 2022), the highest level since the Pliocene (Haywood et al., 2016).

Geological storage involves capturing CO_2 from industrial sources and injecting it into suitable underground geological formations (Bachu, 2003; Bachu et al., 1994; Bachu and Gunter, 2005; Burruss et al., 2009; Kharaka et al., 2006; Pearce et al., 2021; Shukla et al., 2010; Stephenson et al., 2019; Underschultz et al., 2011). Sedimentary basins contain geological media that can be favorable for CO_2 storage and/or sequestration (Cao et al., 2020; Gentzis, 2000) because they typically possess sufficient void space (porosity) and injectivity potential (permeability) and intervening impermeable layers prevent CO_2 from returning to the atmosphere on human timescales (i.e., >1,000 years). Subsurface CO_2 sequestration in sedimentary basins has been accomplished or proposed in depleted oil and gas reservoirs (Herzog, 2001; Jenkins et al., 2012), unmineable coal seams (Shi and Durucan, 2005), caverns in salt structures (Gentzis, 2000), abandoned mines, deep saline aquifers (Bachu and Adams, 2003; Celia et al., 2015; Nordbotten et al., 2005) and freshwater aquifers (Bradshaw et al., 2011; La Croix et al., 2020).

Geological storage of CO_2 is typically employed in regions with significant hydrocarbon production for several reasons (Lane et al., 2021). First, hydrocarbons are more buoyant than water and accumulate in traps (stratigraphic and structural) that remain stable for hundreds of thousands to millions of years. Consequently, buoyant CO_2 should remain safely sequestered if injected into depleted hydrocarbon traps. Second, the geological structures and physical properties of most hydrocarbon fields are well-constrained, reducing geological uncertainty. Finally, existing infrastructure and wells can be repurposed for CO_2 storage operations (Anderson et al., 2005; Garnett et al., 2019). The limited adoption of CCS in areas with no oil and gas exploitation is commonly due to assumptions that suitable underground storage options do not exist or are uneconomic.

Saline aquifers have emerged as primary target reservoirs for several large-scale CCS projects (Ang et al., 2022; Pruess et al., 2003; Shi and Durucan, 2005; Spellman, 2014) and are recognized as having the greatest long-term potential for CCS globally. The estimated CO_2 storage capacity of deep saline aquifers globally

ranges from 400 to 10,000 gigatons (Gt), which is significantly greater than annual global emissions (35–50 Gt; IEA, 2021; Ismail and Gaganis, 2023; Pachauri et al., 2014). In contrast to depleted hydrocarbon reservoirs and coal seams, deep saline aquifers are widely distributed and thus are more likely to be situated near anthropogenic CO_2 sources (Cao et al., 2020). The suitability of saline aquifers for CCS depends on a combination of factors, including total reservoir capacity, leakage potential, injectivity, and potential environmental and human health risks (Celia et al., 2015).

The success of CCS projects depends largely on the suitability of the geological formations selected for CO_2 storage. The first step in identifying a suitable target for CCS is to conduct a regional-scale assessment to identify appropriate horizons and areas for CCS implementation (Bachu, 2003). Regional assessments must account for local geological and hydrogeological conditions (Bachu, 2015), and for saline aquifers, physical and chemical conditions must also be considered (Hitchon, 1996). In this paper, we compile available data on reservoir conditions for sedimentary strata below the LMBC and discuss the implications of these data for further evaluation of CCS potential in the region.

2. Lower Mainland of British Columbia

The Lower Mainland of British Columbia, Canada, is situated in the southeast region of the Georgia Basin and encompasses Metro Vancouver, the Fraser River Lowland, and adjacent mountainous terrain; it is bound by the Coast Mountains to the north, the Cascade Mountains to the east, and the Canada–USA international border to the south. The LMBC is home to more than 60% of British Columbia's population (>3 million people) and is the third-largest urban region in Canada. The LMBC accommodates significant industrial activity with several large carbon emitters, including (in 2023) a refinery, a waste-to-energy facility, and two cement plants (Fig. 3; National Oceanic and Atmospheric Administration, 2022).

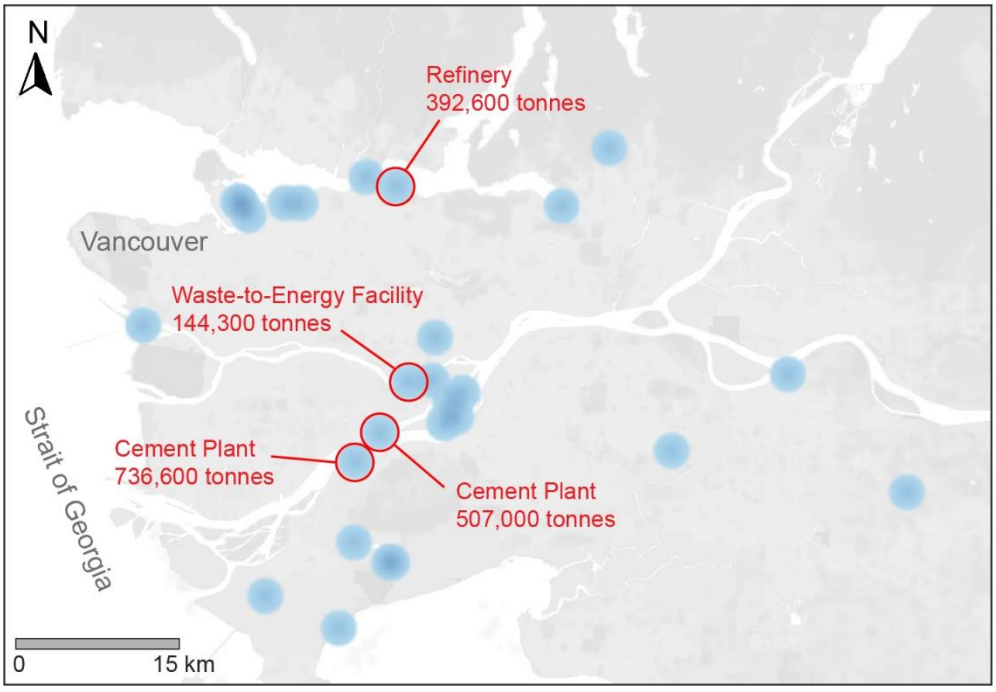

Figure 3 (one column) – Location of major abiogenic CO_2 emissions in LMBC. The approximate annual emissions of the four largest abiogenic CO_2 emitters are shown (Ministry of Environment and Climate Change Strategy, 2023).

2.1 Geology of the Georgia Basin below LMBC

The Georgia Basin is a Cretaceous to Recent forearc basin situated at the boundary between the Insular Superterrane and the Coast Plutonic Complex of the Canadian Cordillera (England, 1991; England and Bustin, 1998; Monger and Price, 2002). The Georgia Basin encompasses the Strait of Georgia, eastern Vancouver Island, Fraser River Lowland, and northwestern Washington State, USA (Fig. 2A; Molnar et al., 2009). The Cretaceous to Neogene fill of the Georgia Basin comprises five outcrop areas (OA) / sub-basins (SB), including: Nanaimo OA, Comox OA, Cowichan Valley OA, Whatcom SB, and Chukanut SB (Fig. 2B; England and Bustin, 1998; Girotto, 2022; Hannigan et al., 2001; Huang et al., 2022; Huang et al., 2019; Kent et al., 2020; Mustard and Monger, 1994). The five OAs / SBs are defined based on the areal extent of Cretaceous and Paleogene outcrops, and the transition between areas in the subsurface has not been defined. The LMBC is situated in the Whatcom Sub-Basin (Fig. 2B), and the Whatcom Sub-Basin is separated from the Chuckanut Sub-Basin by the SW–NE trending Lummi Island Fault (Johnson, 1985; Miller and Misch, 1963).

The basement of the Georgia Basin below the LMBC comprises both the Coast Plutonic Complex, which is a middle Jurassic to Eocene continental arc (Monger and Journeay, 1994), and the Gambier Group, which is a sequence of Lower Cretaceous volcanogenic sedimentary and volcaniclastic rocks that form part of

Wrangellia (Fig. 4; Lynch, 1992; Lynch, 1991; Monger and Journeay, 1994). The Georgia Basin fill below the LMBC comprises siliciclastic strata that include (from bottom to top): Nanaimo Group (mainly Upper Cretaceous), Huntingdon Formation (Fm; Paleocene to Oligocene), Boundary Bay Fm (mainly Miocene), glacial sediment (Quaternary), and Holocene to Recent Fraser River Delta sediments (Figs. 4 and 5; Zelt et al., 2001). The Nanaimo Group was deposited mainly during the Upper Cretaceous to the lowermost Paleocene (England and Bustin, 1998; Huang et al., 2022; Mustard, 1991; Mustard, 1994). The Huntingdon Fm and equivalent Chuckanut Fm disconformably overlie the Nanaimo Group (England and Hiscott, 1992; Hannigan et al., 2001; Johnson, 1991; Johnson, 1984, 1985; Mustard and Monger, 1994) and the Boundary Bay Fm disconformably overlies the Huntingdon Fm (Hopkins Jr, 1968; Hopkins, 1966; Mustard and Rouse, 1991; Mustard, 1994; Rouse et al., 1990). The Boundary Bay Fm is exposed mainly in scattered outcrops along the lower Fraser River Valley and east and northeast of Bellingham in Washington State, USA (Hannigan et al., 2001). Herein, the Huntingdon Fm and Boundary Bay Fm are collectively called Tertiary strata (Fig. 5).

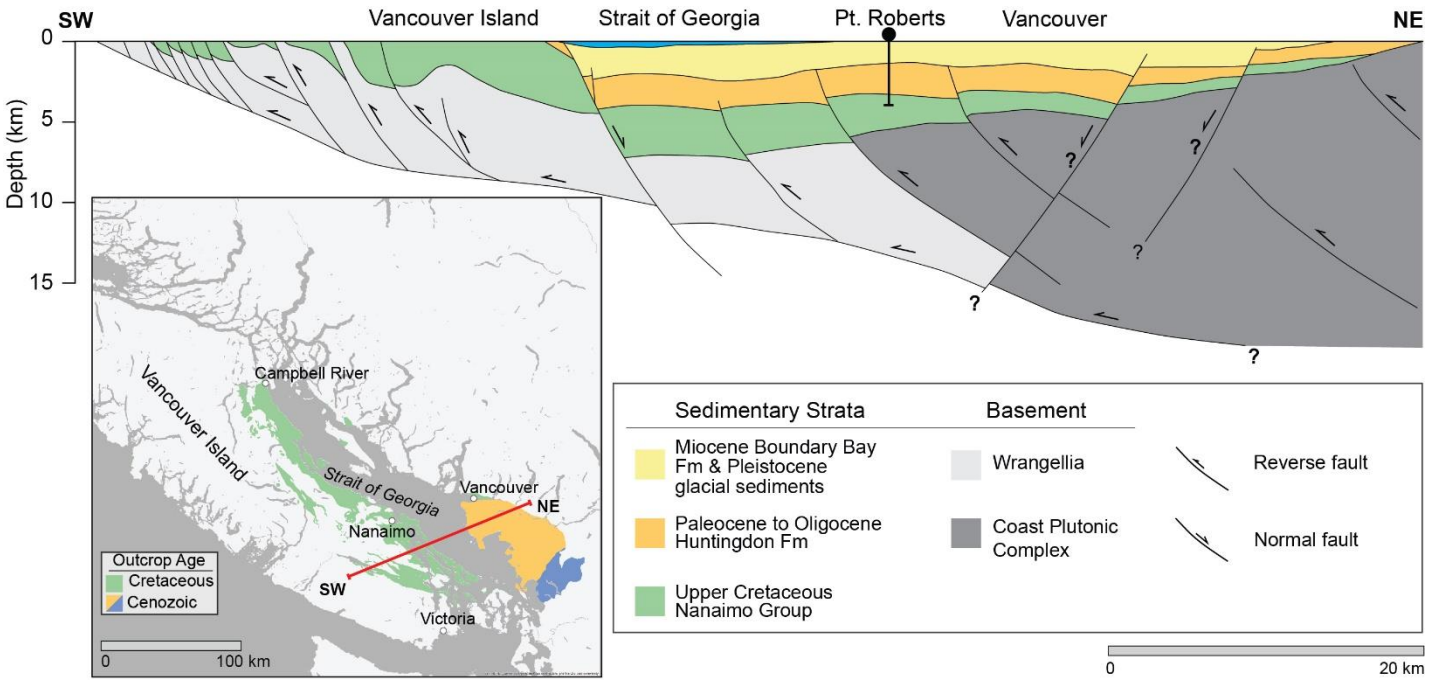

Figure 4 (two columns) – Simplified structural cross-section of the southern Georgia Basin based on LITHOPROBE data (modified after England and Bustin, 1998). Question marks along fault surfaces indicate interpreted locations. Abbreviations: northeast (NE), southwest (SW), formation (Fm).

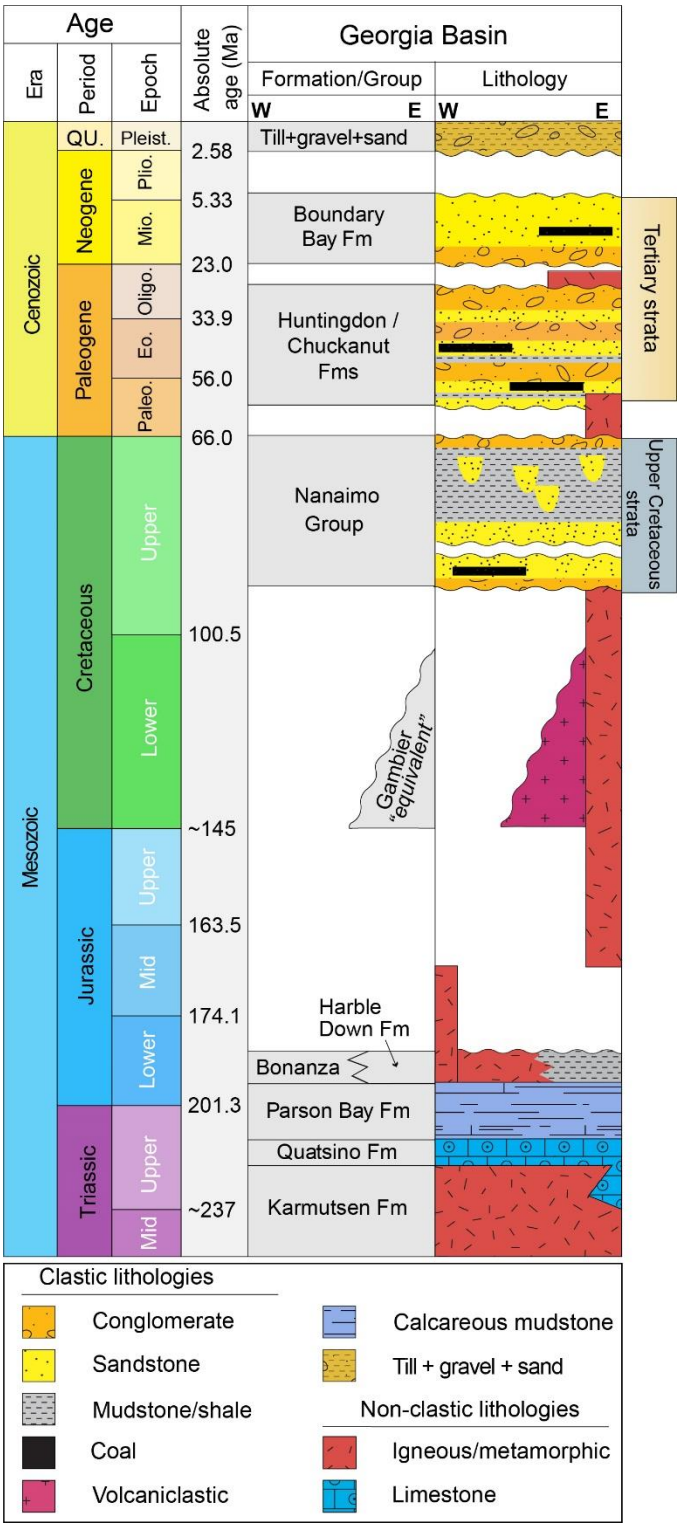

Figure 5 (one column) – Simplified chronostratigraphic column for the Georgia Basin (with data from Bain and Hubbard, 2016; Englert et al., 2018; Haggart, 1992, 1993; Hannigan et al., 2001; Huang et al., 2022; Huang et al., 2019; Kent et al., 2020). Potential reservoir strata include sandstone, conglomerate, and coal seams in the Huntingdon and Boundary Bay formations (Tertiary strata) and sandstone and conglomerate in the Nanaimo Group (mainly Upper Cretaceous strata).

1.2 *Exploration and geophysical studies in LMBC and NW USA*

The Georgia Basin has been studied extensively over the past 170 years, especially on Vancouver Island. Between 1850 and the early 1900s, exploration was spurred by the discovery of sizable bituminous coal resources, which helped fuel the shipping industry. In the early 1900s, exploration for hydrocarbons began (Bustin, 1995; Bustin and England, 1991), and these efforts focused mainly in the LMBC. The first petroleum exploration well was drilled in 1901 in Whatcom County, Washington, USA, and the first well in Canada was drilled in 1906 in the Fraser Valley (Johnston, 1923; McFarland, 1983). While 118 oil and gas exploration wells have been drilled in the Whatcom Sub-Basin of the Georgia Basin (Hannigan et al., 2001), only 11 wells in the Canadian extent of the sub-basin have available geophysical log data (Table 1; Fig. 6). A considerable proportion of wells drilled in LMBC and NW USA are relatively shallow (<300 m deep), and may have been drilled as water wells (Hannigan et al., 2001).

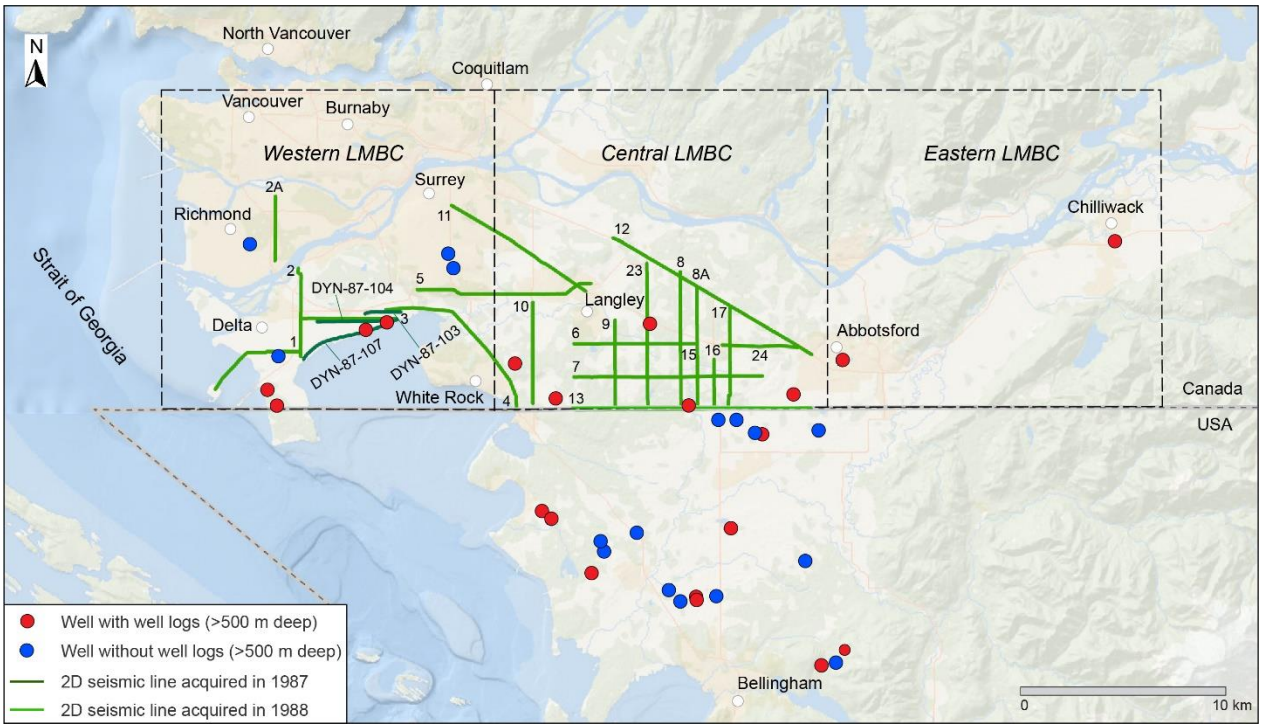

Figure 6 (two columns) – Location of wells (>500 m depth) drilled in the LMBC and northwest Washington State, USA, and available 2D seismic lines in the LMBC. 2D lines in light green were acquired in 1988, and 2D lines in dark green were acquired in 1987. The Western LMBC, Central LMBC, and Eastern LMBC (squares with dashed lines) are referred to in the text.

Unique well identifier (UWI)	Latitude	Longitude	Rig release (dd-mm-yyyy)	Ground elevation (m)	Kelly bushing (KB) (m)	Total depth (m)	Cores (No. of cores: cored interval (total core length))	Well logs
Canada								
D-095-D/092-G-02	49.07943	-122.93089	02-10-1991	0.5	5.5	1,700.0	1: 940.4 – 958.4 (18 m total)	GR | CAL | N | DEN | PE | SON | RES | SP
B-051-C/092-G-02	49.04302	-122.75953	08-04-1962	109.7	113.6	3,322.0	7: 1,393.3 – 3,321.1 (50.1 m total)	GR | SON | RES | SP | CO
C-011-D/092-G-01	49.01451	-122.38697	24-08-1959	40.2	42.4	2,396.3	1: 2,369.5 – 2,372 (2.5 m total)	GR | CAL | N | RES | SP
B-056-C/092-G-01	49.04315	-122.32168	05-01-1962	66.1	70.1	958.6	1: 957.4 – 958 (0.6 m total)	GR | SON | RES | SP | CO
A-017-B/092-G-02	49.01217	-122.70506	14-10-1957	26.2	29.0	1,585.6	8: 1,271 – 1,568.8 (30.6 m total)	CAL | RES
D-007-A/092-G-03	49.00791	-123.08117	25-01-1963	55.1	60.7	4,508.6	7: 1,248.2 – 4,508.7 (51.3 m total)	GR | CAL | N | SON | RES | SP
D-077-E/092-H-04	49.00628	-123.07756	30-09-1964	10.7	11.3	1,885.8	2: 1,231.4 – 1,381.1 (12.2 m total)	GR | SON | RES | SP | CO
A-028-A/092-G-03	49.02038	-123.09069	05-09-1955	61.3	63.4	1,842.2	No	RES
C-087-D/092-G-02/2	49.07316	-122.95907	27-06-1995	1.0	4.7	1,270.0	No	GR | CAL | N | DEN | PE | RES | SP
A-097-A/092-G-02	49.07764	-122.57824	02-11-1993	85.2	91.5	2,635.0	No	GR | CAL | SON | RES | SP
D-003-A/092-G-02	49.00541	-122.52643	20-09-1993	50.0	56.3	2,432.0	No	GR | CAL | SON | SP
USA (Rig Release dates are approximate | *Italicized* values are estimates)								
5-39N-1E (W-72)	48.905	-122.711	*12-11-1945*	43.8	-	1,899.2	?	RES | SP
23-39N-1E (431)	48.858	-122.658	*09-11-1991*	73.4	78.9	1,831.4	Side wall core	GR | CAL | SON | RES | N | DEN | SP
26-39N-2E (432)	48.835	-122.517	*14-11-1991*	27.4	32.9	1,347.5	Side wall core	GR | CAL | SON | RES | N | DEN | PE | SP
4-40N-3E (166)	48.979	-122.428	*20-10-1972*	37.1	40.2	2,556.1	No	GR | CAL | N | SON | RES| SP | CO
18-38N-4E (235)	48.775	-122.352	*13-05-1969*	163.9	167.0	1,883.6	No	GR | CAL | N | DEN | RES | SP | CO
26-39N-2E (457)	48.835	-122.517	*13-05-1998*	27.4	27.4	560.8	Yes	GR | CAL | N | DEN | SON | RES | SP | CO
32-40N-1E (420)	48.913	-122.723	*11-06-1990*	23.4	27.4	2,781.6	No	GR | CAL | DEN | PE | SON | RES | SP | CO
17-38N-4E (170)	48.777	-122.331	*10-11-1962*	211.8	214.2	1,434.6	Yes	CAL | RES | SP | SON | CO
6-39N-3E (W-74)	48.896	-122.471	*24-01-1948*	19.8	-	1,064.3	?	RES | SP

Table 1 (two columns) – Available drill, core, and geophysical well logs for the 11 wells in the LMBC and 9 wells in northwest Washington State, USA, that have well logs. In the "cores" column, the cored interval indicates the upper and lower bounds of the interval in which cores were collected, but core coverage is intermittent within that interval. Well-log acronyms: Photoelectric (PE); Spontaneous Potential (SP); Gamma Ray (GR); Caliper (CAL); Sonic (SON); Neutron (N); Density (DEN); Resistivity (RES); Conductivity (CO).

Since the early 1920s, various exploration surveys have been conducted, including geological, seismic, gravimetric, and magnetic surveys. In 1955, a regional aeromagnetic survey was acquired from across the Georgia Basin. In 1959, a gravity survey was acquired over most of the Fraser Valley and west of Abbotsford. In the same year, the first large-scale seismic reflection survey was collected between Abbotsford and the Strait of Georgia and between the Fraser River and the United States border. Between 1977 and 1988, a series of 2D seismic surveys were acquired across the LMBC to assess gas storage potential and hydrocarbon prospectivity. Of these surveys, only 322 km of 2D lines remain available in

digital format (Fig. 6). In 1987, an additional 160 line-km of 2D seismic lines were acquired close to the Canada-USA border in Whatcom County, USA.

3. CO_2 storage mechanisms and fundamentals in deep-saline aquifers

3.1 Subsurface CO_2 storage mechanisms

The feasibility of sequestering CO_2 in subsurface aquifers is controlled, in part, by the properties of CO_2 gas (Hassanzadeh et al., 2009). Specifically, at temperatures greater than 31.1°C and pressures greater than 7.38 MPa (critical point), CO_2 enters a supercritical state, and this typically occurs at a subsurface depth of approximately 800 m (Figs. 7 and 8). Supercritical CO_2 behaves as a gas but has a high density that typically increases from ~350 kg m^{-3} to over ~700 kg m^{-3} between ~800 and 2,000 m (Fig. 7). Subcritical CO_2 can exist in either gaseous or liquid states, depending on temperature and pressure conditions. CO_2 is liquid at temperatures below 31.1°C and pressures above 7.38 MPa. The efficient storage of CO_2 in a supercritical or liquid state is aided by its high density, which reduces buoyancy forces and allows for more effective use of available pore space (Fig. 8; Cao et al., 2020; Hassanzadeh et al., 2009; Hileman, 1997).

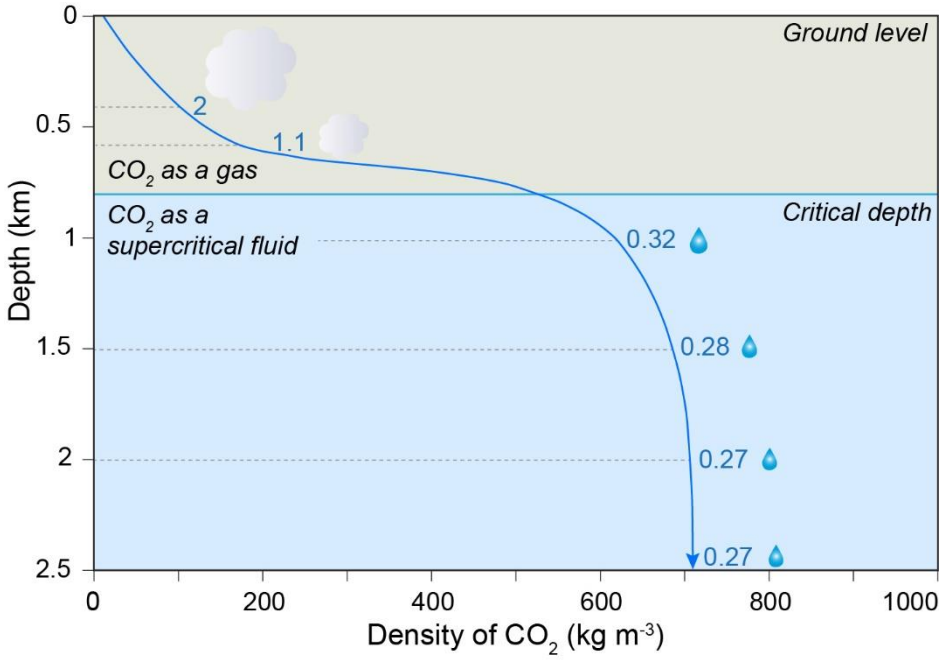

Figure 7 (one column) – Density variation of CO_2 with depth and assuming a hydrostatic pressure for freshwater (9.81 MPa km^{-1}), a geothermal gradient of 25 ^oC km^{-1}, and a surface temperature of 15°C. CO_2 density increases rapidly between approximately 600 m and 800 m depth, after which it reaches a supercritical state. Cloud (CO_2 in a gaseous state) and droplet (CO_2 in a supercritical or liquid state) images are schematic only and reflect the relative volume occupied by the CO_2 at different subsurface depths; the relative volumes are provided by the numbers next to the cloud

and droplet images. At depths below 1.5 km, density and specific volume become nearly constant (modified after Angus et al., 1974).

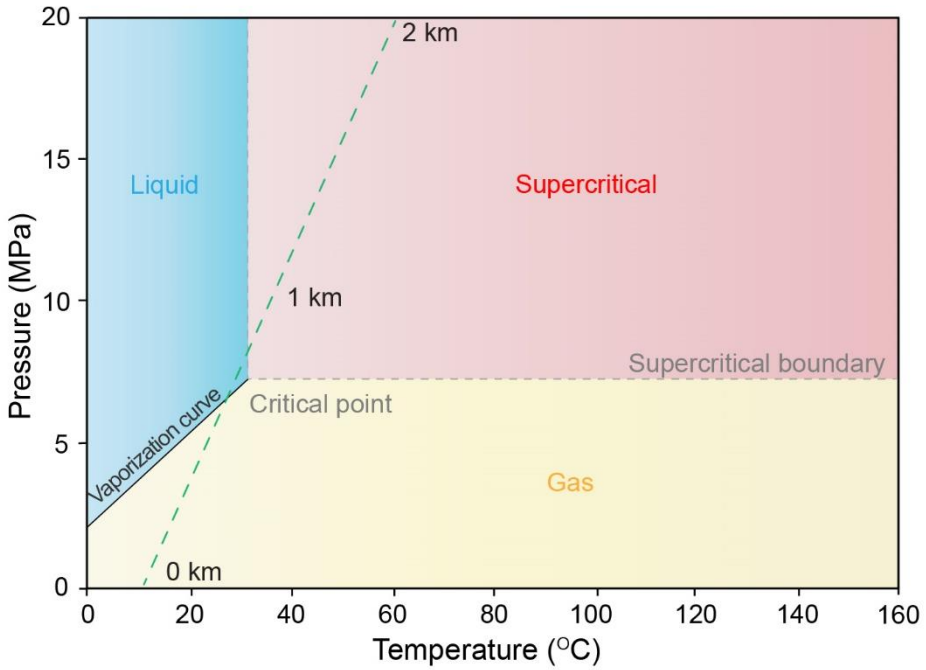

Figure 8 (one column) – Phase diagram of CO_2 (modified after Bachu, 2000; Bachu, 2003; Jafari et al., 2017). The 1 km and 2 km depths are based on freshwater hydrostatic pressure, a geothermal gradient of 25 °C km^{-1}, and an average surface temperature of 11 °C (LMBC average surface temperature).

Various mechanisms contribute to the sequestration of CO_2 in aquifers, including structural/stratigraphic trapping, residual trapping, mineral trapping, and solubility trapping (Fig. 9; De Silva et al., 2015; Emami-Meybodi et al., 2015). Structural/stratigraphic trapping involves the confinement of CO_2 in the pores of water-saturated sedimentary media below impermeable barriers (e.g., caprock; Fig. 9). Through this trapping method, CO_2, typically in a supercritical state, is injected into a saline aquifer that is overlain by a caprock. Due to the difference in density between the supercritical CO_2 (~350 kg m^{-3} to over 700 kg m^{-3}) and host brine (1,000–1,300 kg m^{-3}), the CO_2 rises buoyantly and becomes trapped below the caprock (Ang et al., 2022). Different types of traps, such as anticline, fault, lithological, and unconformity traps, are considered suitable for structural/stratigraphic trapping, and the distribution of CO_2 within these traps is primarily influenced by factors such as viscosity, capillary forces, and gravity (Ang et al., 2022; Na et al., 2015; Zhang and Song, 2014). The effectiveness of tight, low-permeability caprock and confining layers in preventing the escape of CO_2 is primarily a function of their high capillary force (Rosenbauer and Thomas, 2010). If the saline aquifer is unconfined, positively buoyant CO_2 can migrate from the injection site to other reservoirs, including freshwater aquifers, and ultimately to surface and back into the atmosphere. The upward buoyancy of CO_2 in a saline aquifer is directly related to the CO_2-brine density difference and formation permeability. The capillary forces of the caprock determine the pressure at which the caprock is

breached (Ang et al., 2022). When the buoyancy force of the CO_2 column exceeds the capillary threshold of the caprock, the supercritical fluid can penetrate the caprock and form cracks (fractures) within it (Iglauer, 2018).

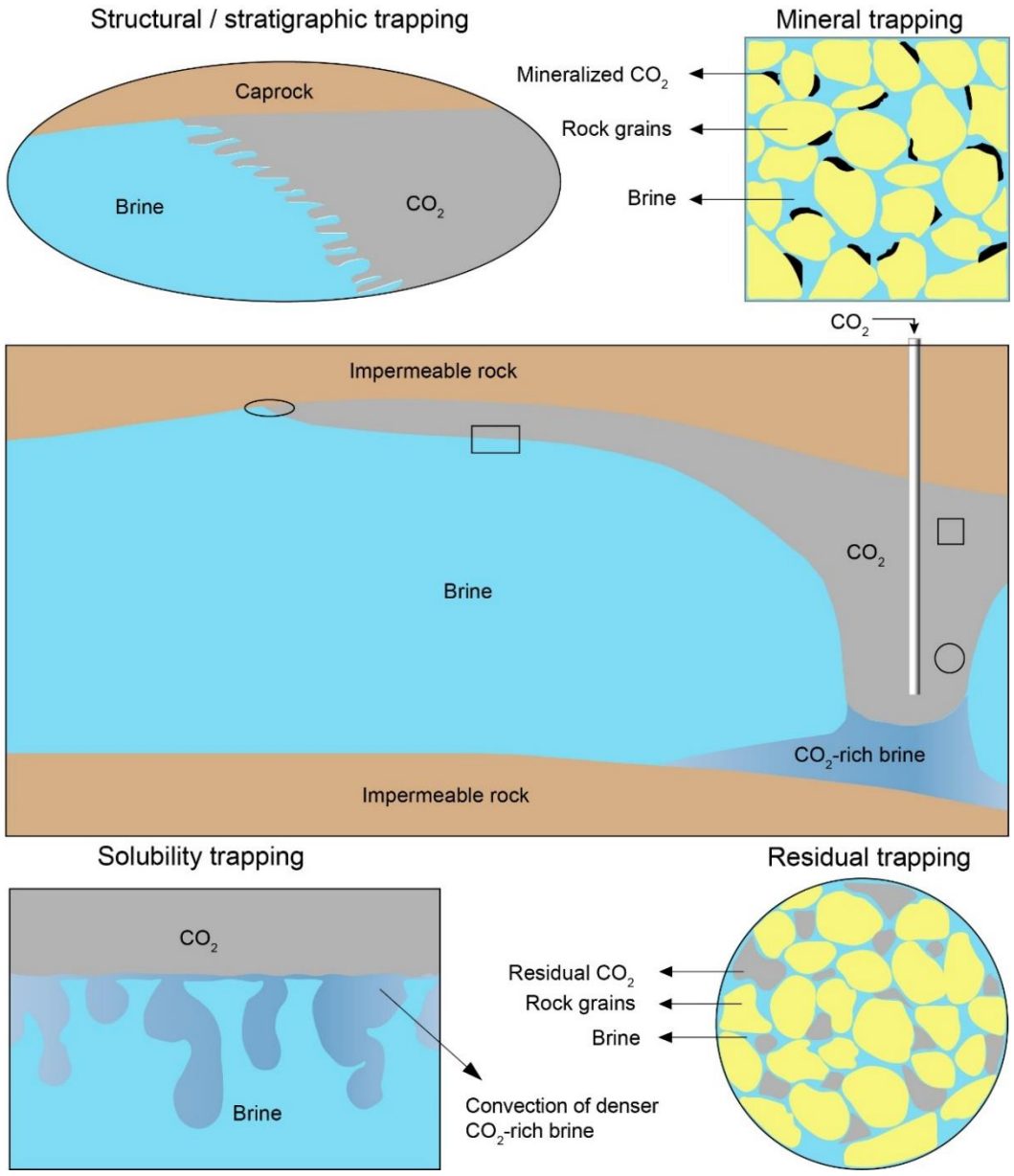

Figure 9 (1.5 column) – Simplified illustration of fluid dynamics and trapping mechanisms attributed to geological sequestration of CO_2 in saline aquifers. The shapes of the four polygons in the middle figure relate to the closeup images above and below the main figure (modified after Emami-Meybodi et al., 2015).

Residual trapping refers to the sequestration of injected CO_2 by capillary forces in the pores of reservoir rocks (Fig. 9), and it is an important CO_2 storage mechanism with a high degree of long-term storage safety (Jafari et al., 2017; Kumar et al., 2020). Residual trapping occurs when brine backfills the trailing edge of a mobile plume of supercritical CO_2 that itself displaces the resident fluid. As the buoyant CO_2 plume migrates through the formation, saline water partially replaces it, and some CO_2 is left behind as disconnected/residual droplets in the pore spaces (Benson and Cole, 2008). The magnitude of residual saturation in a rock and the fraction of injected CO_2 that can be stored in this form depends on the pore network geometry in the host rock (Rosenbauer and Thomas, 2010). The degree of residual trapping ranges from 15–25% for typical saline aquifers but can exceed 25% depending on the porosity and permeability of the formation (Fig. 10; Holtz, 2002; Juanes et al., 2006; Kumar et al., 2005).

Solubility trapping occurs when injected CO_2 dissolves in formation water (Fig. 9; Bachu and Adams, 2003; Hassanzadeh et al., 2009). The solubility of CO_2 is influenced by various factors, including contact area, contact time, reservoir temperature and pressure, salinity, and brine composition (Hassanzadeh et al., 2005). The solubility of CO_2 generally decreases with increasing temperature and salinity but increases with increasing pressure (Spycher and Pruess, 2005). In saline aquifers, the dissolution of CO_2 in formation water and the resulting increase in density of the CO_2-rich brine beneath a caprock or sealing formation results in a density gradient that initiates natural convection, leading to the enhanced dissolution of CO_2 (Bachu et al., 1994; Cao et al., 2020; Ennis-King et al., 2005; Hassanzadeh et al., 2007; Pruess et al., 2003); this increases the longer-term effectiveness of CO_2 sequestration by preventing the escape of buoyant CO_2 (Hassanzadeh et al., 2009). Nevertheless, under typical saline aquifer conditions, natural convection takes hundreds to thousands of years (Fig. 10; Anderson et al., 2005; Hassanzadeh et al., 2009).

Under favorable geological conditions, a portion of injected CO_2 forms carbonate minerals in a process known as mineral trapping (Fig. 9). Mineral trapping is a promising mechanism for the long-term storage of CO_2 as it can significantly increase storage capacity and immobilizes CO_2 permanently (Gunter et al., 1997; Gunter et al., 1993; Pearce et al., 2020; Rosenbauer and Thomas, 2010). However, the precipitation of minerals within host rock pores, particularly in close proximity to the injection site, can severely reduce permeability and impede further injection (Rosenbauer and Thomas, 2010). As well, after mineralization, the pH, ion concentration, and total salinity of the brine change (Ang et al., 2022; De Silva et al., 2015). The effectiveness of mineral trapping in CO_2 geological storage is closely tied to factors such as rock type (carbonate, clastic, evaporite), mineralogy, permeability barriers, and diffusion (Pearce et al., 2021). The dissolution of primary minerals and precipitation of secondary minerals can impact porosity, permeability, and flow behavior, influencing storage efficiency (Piri et al., 2005). Mineral trapping is the most stable method of CO_2 storage but typically requires a long reaction time (Kumar et al., 2020).

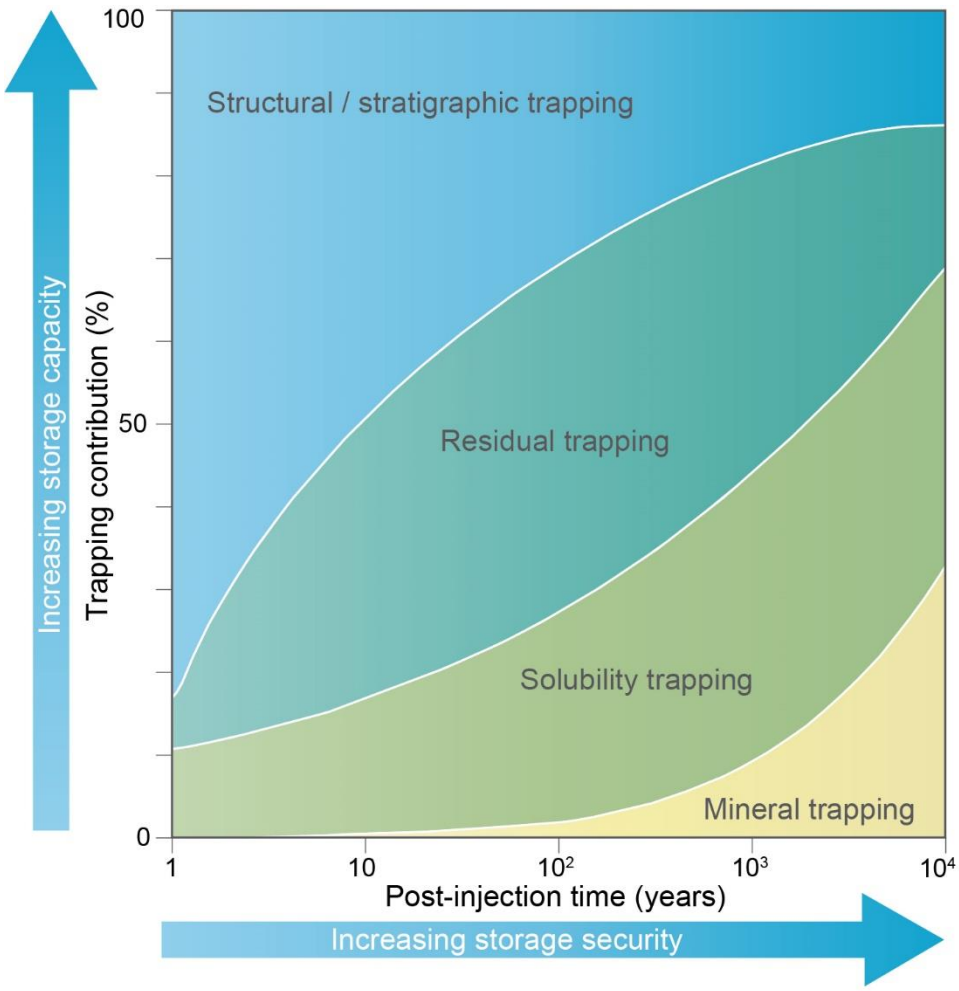

Figure 10 (one column) – Schematic illustration of contribution of various CO_2 trapping mechanisms *versus* post-injection time, including structural/stratigraphic trapping, residual trapping, solubility trapping, and mineral trapping in saline aquifers (after Anderson et al., 2005; Metz et al., 2005). Storage security increases as more CO_2 is sequestered through mineral and solubility trapping.

3.1 Enhanced solubility trapping of CO_2

The injected mobile gaseous/supercritical CO_2 in a saline aquifer is less dense than the resident brine and its buoyancy drives its migration under a confining caprock (Fig. 9). If the caprock is compromised (contains high-permeability fractures or poorly cemented well bores) it will fail to retain buoyant CO_2, and the injected CO_2 will flow upward and escape through high permeability zones (Emami-Meybodi et al., 2015; Hassanzadeh et al., 2005; Hassanzadeh et al., 2009). Once CO_2 is dissolved in formation water (solubility trapping), converted to rock (mineral trapping), or trapped in pores (residual trapping), buoyancy forces become negligible, and the trapped CO_2 remains in the aquifer with minimal risk of leakage (Cao et

al., 2020). Accelerating the dissolution rate of CO_2 in formation water is an effective approach for increasing storage security as it reduces the time available for mobile free-phase CO_2 to escape.

Several methods have been proposed to accelerate CO_2 dissolution in saline aquifers, including water-alternating-gas, *ex-situ* dissolution, and *in-situ* dissolution. Injecting brine following CO_2 injection (water-alternating-gas) significantly reduces dissolution time, potentially causing half of injected CO_2 to dissolve within 200 years (Hassanzadeh et al., 2009; Keith et al., 2005). *Ex-situ* dissolution involves mixing compressed CO_2 and target formation brine at the surface and injecting the CO_2-brine mixture into the subsurface saline aquifer (Fig. 11A; Zendehboudi et al., 2011; Zendehboudi et al., 2012). *Ex-situ* dissolution is an effective CO_2 storage strategy with a relatively low level of uncertainty (Eke et al., 2011; Leonenko and Keith, 2008), but it requires energy to overcome pressure drops in the mixing pipeline and aquifer and power large pumps. High-capacity pumps are needed because the volume of necessary brine in *ex-situ* dissolution is significantly greater than the volume of CO_2 due to the low solubility of CO_2 in brines (approximately 30 kg CO_2 per m^3 of brine; Ang et al., 2022; Cao et al., 2020). The primary benefits of *ex-situ* dissolution are a significantly reduced probability of buoyant CO_2 escape and reduced impact on groundwater resources (Cao et al., 2020). Also, formation water with dissolved CO_2 is denser than formation water, and hence, the CO_2-rich brine is negatively buoyant (Emami-Meybodi et al., 2015; Hassanzadeh et al., 2009). The primary disadvantages of *ex-situ* dissolution are greater capital and operational costs (Burton and Bryant, 2009) and the need to extract and inject large volumes of brine.

In-situ dissolution (or downhole dissolution) also enhances solubility trapping of CO_2 in saline aquifers (Zirrahi et al., 2013). In *in-situ* dissolution, CO_2 and brine are injected simultaneously into the wellbore. A static mixer is used as a mass transfer device to mix them at the bottom of the well (Fig. 11B). *In-situ* dissolution has the same advantages as *ex-situ* dissolution (i.e., reduced probability of escape of buoyant CO_2 and reduced impact on groundwater resources), but also avoids exposing the entire wellbore and surface facilities to the corrosive solution of CO_2 and brine. Additionally, *in-situ* dissolution causes higher solubility of CO_2 in brine at higher downhole pressures and requires less energy for CO_2 compression (Emami-Meybodi et al., 2015).

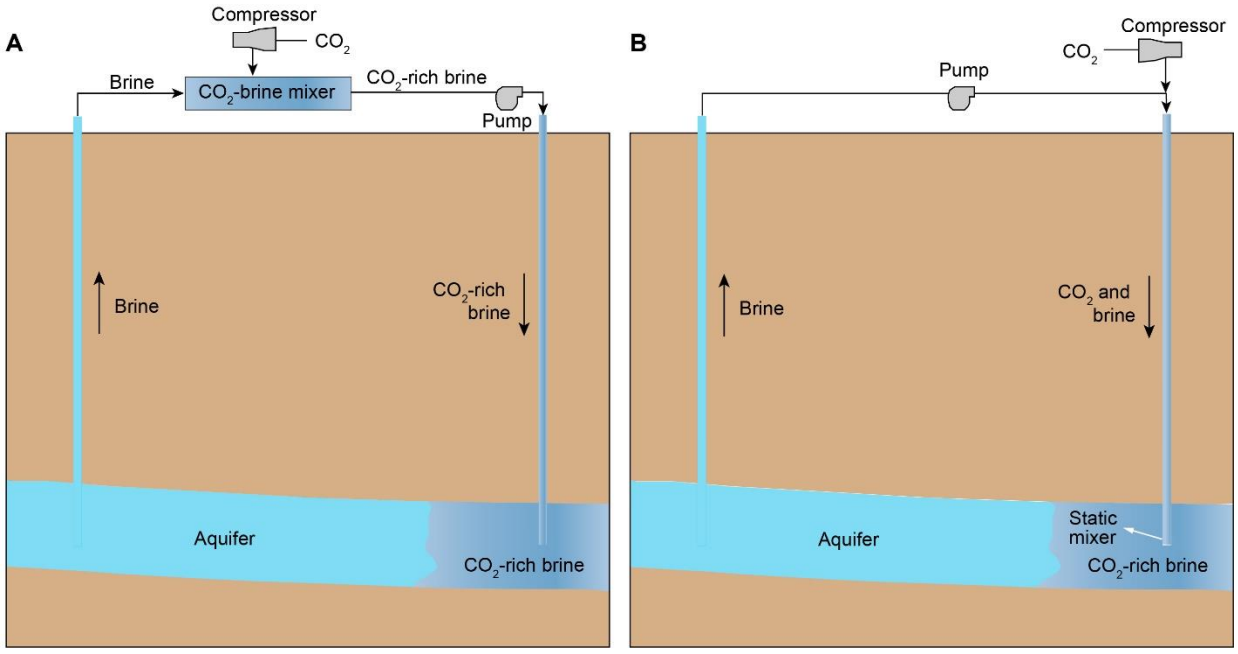

Figure 11 (two columns) – Schematic illustrations of A) *ex-situ* and B) *in-situ* dissolution designs for enhancing solubility trapping of CO_2 in saline aquifers (modified after Emami-Meybodi et al., 2015).

4. Favorable characteristics for CO_2 sequestration in saline aquifers with data from the LMBC

Ideal basins for gaseous/supercritical CO_2 storage are water-saturated and permeable sedimentary strata (reservoirs) overlain by laterally extensive layers of low-permeability rocks (caprock) that are structurally simple (Keighley and Maher, 2015). Structurally simple basins contain few laterally and vertically continuous faults and typically occur in mid-continent positions (e.g., Western Canada Sedimentary Basin). Basins located in tectonically active areas (e.g., Georgia Basin) are less suitable for gaseous/supercritical CO_2 storage largely because they are more structurally complex with through-going faults that may act as potential pathways for buoyant CO_2 escape (Anderson et al., 2005; Chiodini et al., 2001; Granieri et al., 2003). In tectonically active basins, other viable CO_2 sequestration mechanisms, such as *in-situ* and *ex-situ* dissolution and injection in deep saline aquifers or coal seams, are more secure approaches for mitigating the risk of CO_2 leakage or groundwater contamination.

Reservoir rocks for underground CO_2 storage include micro-fractured coal (Gentzis, 2000) and porous and permeable sandstone, limestone, and dolomite. Seals include evaporites (e.g., anhydrite, salt) and fine-grained clastic rocks (e.g., mudstone; Keighley and Maher, 2015). Below the LMBC, the mainly Upper Cretaceous Nanaimo Group (Figs. 4 and 5) comprises thick intervals dominated by sandstone and/or conglomerate that are situated within and between regionally extensive mudstone intervals (Bain and

Hubbard, 2016; England and Bustin, 1998; Englert et al., 2018; Huang et al., 2022; Kent et al., 2020). The Paleocene to Oligocene Huntingdon Fm is interpreted as a thick sequence of fluvial and associated terrestrial strata dominated by sandstone with lesser conglomerate and laterally discontinuous mudstone (Mustard, 1994). Coal seams regularly occur throughout the interval (Gilley, 2003). The Miocene Boundary Bay Fm consists of varying amounts of interbedded sandstone, mudstone, conglomerate, and coal (Fig. 5; Gordy, 1988; Hannigan et al., 2001; Mustard, 1994).

Below, we discuss the key characteristics of sedimentary basins and sedimentary strata required for CO_2 storage in tectonically active regions. Key characteristics include geothermal gradient and pressure, reservoir depth and thickness, salinity, mineralogy, porosity-permeability, seismicity, and faults. We also summarize and present information on these characteristics from the Georgia Basin and below the LMBC.

4.1 Geothermal gradient and pressure

Geothermal gradient and pressure impact the phase behavior of CO_2 (Bachu, 2003; Bachu and Adams, 2003), which determines the effective storage and dissolution of CO_2 (Keighley and Maher, 2015). Under normal hydrostatic pressure gradients and a geothermal gradient of 25 $^{o}C\ km^{-1}$, CO_2 reaches a supercritical state at about 800 m depth (Fig. 8; Holloway and Savage, 1993); however, the depth at which CO_2 reaches liquid and supercritical conditions varies as a function of surface temperature, local geothermal gradient, and local hydrostatic and lithostatic pressures (Bachu, 2003). For example, in the Western Canada Sedimentary Basin, the critical point ranges from <800 m in the north, where geothermal gradients reach 50 $^{o}C\ km^{-1}$, to >1,200 m in the south, where geothermal gradients are around 20 $^{o}C\ km^{-1}$ (Bachu, 2003)

The relationship between hydrostatic pressure and depth is described by:

$$P = \rho_w \cdot g \cdot z \qquad \text{[EQ. 1]}$$

where P is the hydrostatic pressure, ρ_w is formation water density, g is the gravitational constant, and z is the depth below surface. Equation 1 indicates that hydrostatic pressure increases with depth in a fluid column due to the weight of the overlying fluid. In most sedimentary basins, pressure conditions are either hydrostatic or very nearly so.

Temperature variations with depth can be calculated using Equation 2 and using the average surface temperature (T_s) and geothermal gradient (GG):

$$T = T_s + GG \cdot z \qquad \text{[EQ. 2]}$$

Surface temperatures in sedimentary basins exhibit considerable variation worldwide, with basins in arctic and sub-arctic regions experiencing average surface temperatures around 0°C (possibly dropping to -2°C near permafrost and glaciers) and basins in low-altitude tropical regions experiencing surface temperatures of approximately 30°C (Bachu, 2003). By combining Equations 1 and 2, it is possible to determine the phase state of CO_2 in a sedimentary basin (EQ 3; Bachu, 2003):

$$P = \frac{(\rho_w \cdot g) \cdot (T - T_S)}{GG} \qquad \text{[EQ. 3]}$$

Assuming a freshwater hydrostatic pressure gradient and geothermal gradients ranging from 20–60 °C km^{-1}, an envelope can be constructed to predict the phase behavior of CO_2 in sedimentary basins (Fig. 12). In basins with high geothermal gradients (GG >40 $^oC\ km^{-1}$; Bachu, 2003) and with increasing depth (changing P–T conditions), CO_2 gas transitions directly into a supercritical fluid (Fig. 12), and there is a correspondingly rapid increase in CO_2 density (Fig. 13). With increasing depth in high-GG basins, temperature effects limit density increases induced by raising pressure and this results in a much more modest increase in density with depth (Fig. 13). In basins with low geothermal gradients (GG <30 $^oC\ km^{-1}$) and with increasing depth CO_2 gas transitions into a liquid first and then a supercritical fluid (Fig. 12). For liquid CO_2, the influence of temperature on density outweighs that of pressure (Bachu, 2003), and hence, in many instances the density of CO_2 decreases with increasing depth or remains nearly constant (Fig. 13). The maximum attainable CO_2 density under normal pressure conditions is approximately 850 kg m^{-3}.

The way CO_2 density changes with depth in high geothermal gradient basins versus low geothermal gradient basins has important implications for both CO_2 storage and behavior. Specifically, the change in CO_2 density with depth in high geothermal gradient basins versus low geothermal gradient basins impacts the minimum depth range for CO_2 storage in its supercritical or liquid phases. The minimum storage depth for liquid or supercritical CO_2 in low geothermal gradient basins ranges from 800–1,000 m and in high geothermal gradient basins it ranges from 1,500–2,000 m (Bachu, 2003).

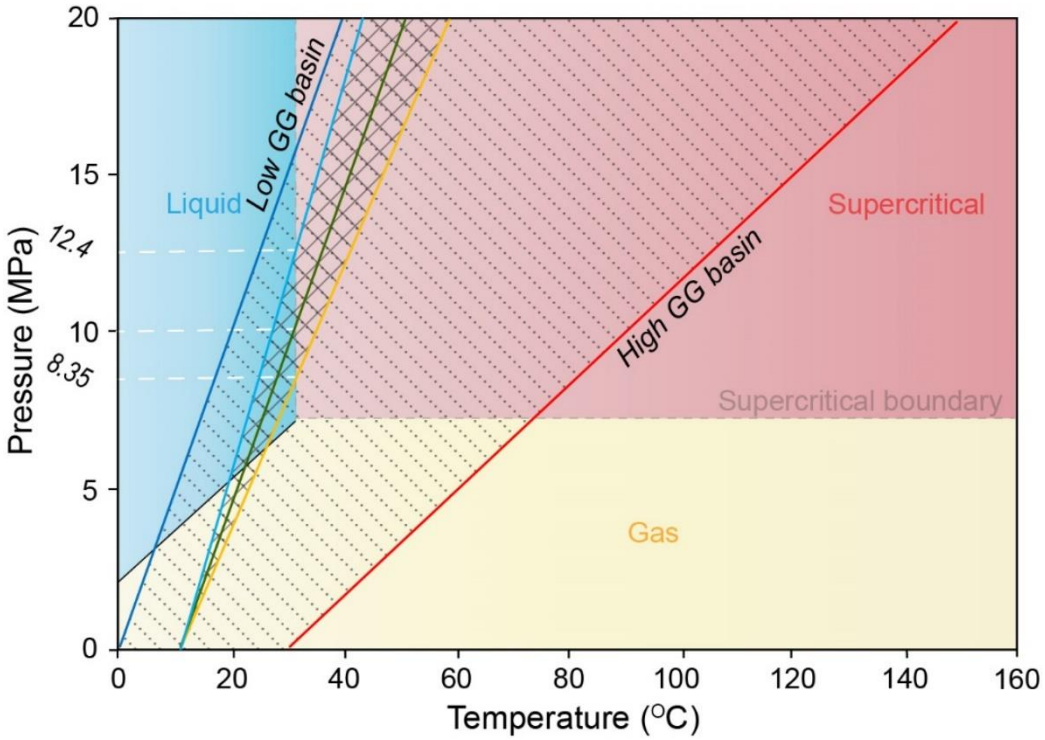

Figure 12 (one column) – Phase behavior of CO_2 for conditions characteristic of sedimentary basins. The area highlighted by the stippled pattern defines the pressure-temperature envelope found in most sedimentary basins globally (modified after Bachu, 2003). The high geothermal gradient basin line reflects a basin with a geothermal gradient of 60 ^{o}C km^{-1} and an average surface temperature of 30^{o}C (tropical conditions). The low geothermal gradient line reflects a basin with a geothermal gradient of 20 ^{o}C km^{-1} and an average surface temperature of 0^{o}C (arctic conditions). The area defined by crosshatched pattern is for the Georgia Basin, Canada, and the blue, green, and orange lines are calculated based on the 5 lowest (16.2 ^{o}C km^{-1}), average (20 ^{o}C km^{-1}), and 5 highest (24 ^{o}C km^{-1}) recorded geothermal gradient in the LMBC and northwest USA. Acronyms: Geothermal gradient (GG).

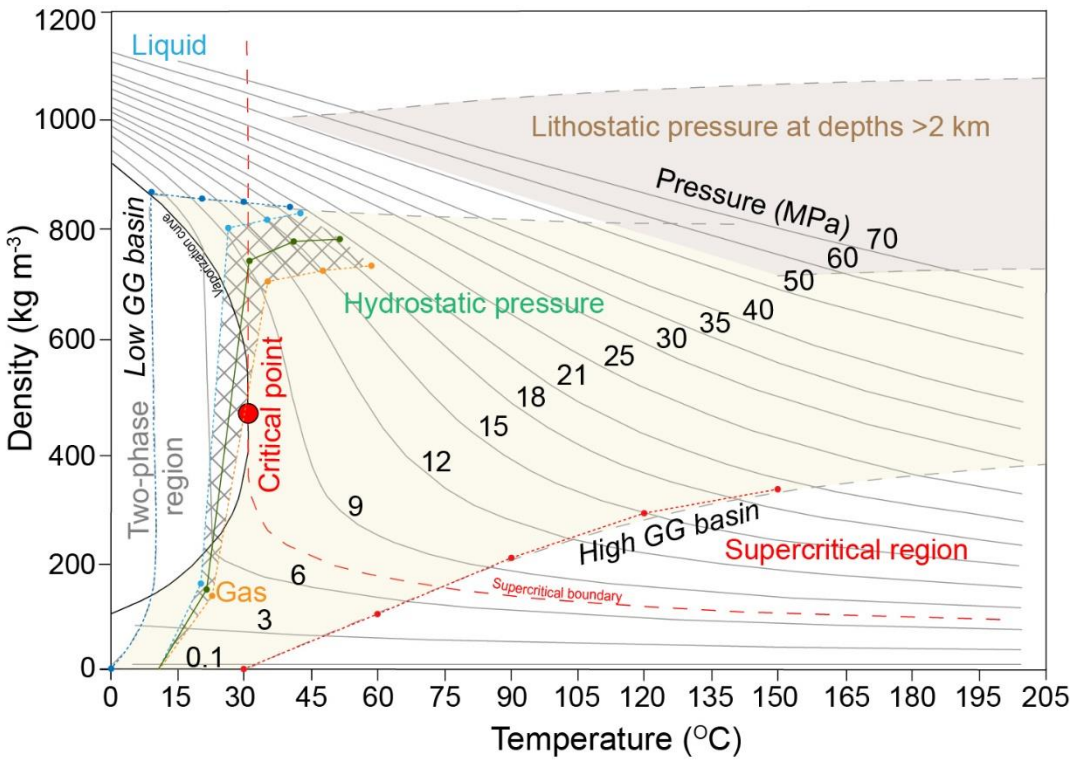

Figure 13 (one column) – Variation in CO_2 density as a function of temperature and pressure (modified after Bachu, 2003). The high geothermal gradient basin line reflects a basin with a geothermal gradient of 60 $^oC\ km^{-1}$ and an average surface temperature of 30°C (tropical conditions). The low geothermal gradient line reflects a basin with a geothermal gradient of 20 $^oC\ km^{-1}$ and an average surface temperature of 0°C (arctic conditions). Cross-hatched area represents the variations of CO_2 density for the lowest (blue dashed line), average (green dashed line), and highest (orange dashed line) recorded geothermal gradient in the LMBC and northwest USA. The data points along the geothermal gradient lines show CO_2 density at 500, 1000, 1500 and 2000 m depth. Acronyms: Geothermal gradient (GG).

In the Georgia Basin and below the LMBC, borehole temperatures are derived from 11 wells using bottom hole temperatures recorded on wireline log headers and drill stem test (DST) reports (Table 2). In northwest Washington State, USA, borehole temperatures are derived from 7 wells using bottom hole temperatures recorded on wireline log headers (Table 2). Reported values are calculated using Equation 4:

$$GG = \frac{(T_b - T_s)}{(Z_b - Z_s)} \qquad \text{[EQ.4]}$$

where T_b is bottom hole temperature from wireline logs or borehole temperatures that are obtained from DSTs (°C), T_s is average surface temperature (°C), Z_b is depth (km) at which the temperature was recorded, and Z_s is ground level (km).

Geothermal gradients calculated from bottom hole temperatures from wireline logs in the LMBC range mainly from 14.6–26.5 $^oC\ km^{-1}$ which is typical of cold basins and favorable for CO_2 sequestration (Table

2; Fig. 14A–B). Multiple bottom hole temperature measurements were recorded at different depths in multiple wells. The highest geothermal gradient from wireline log bottom hole temperatures is recorded in well D-077-E/092-H-04 (average (n=2): 26.5 ^{o}C km^{-1}) in Eastern LMBC, while the lowest geothermal gradient is in well A-017-B/092-G-02 (14.6 ^{o}C km^{-1}) in Central LMBC (Fig. 15). Note that some wells with multiple borehole temperature readings show a geothermal gradient that decreases with depth, and this is perhaps the result of temperature suppression induced during drilling. In the American extent of the Georgia Basin, the geothermal gradient ranges from 18–25.5 ^{o}C km^{-1} (Fig. 15).

Geothermal gradients calculated from temperatures measured during DSTs in the LMBC range from 17.8–27.8 ^{o}C km^{-1} (Table 2; Figs. 14C–D, 16). The well with the highest geothermal gradient determined using DST temperatures is A-097-A/092-G-02 (average (n=2): 26.3 ^{o}C km^{-1}) in Central LMBC, while wells with the lowest geothermal gradient are D-007-A/092-G-03 (17.8 ^{o}C km^{-1}) and C-011-D/092-G-01 (17.9 ^{o}C km^{-1}) in Western LMBC and Central LMBC, respectively. No temperature measurements have been reported from DSTs in wells in northwest Washington State, USA.

Considering the temperature measurements acquired from the LMBC and northwest Washington State, USA, a plausible estimation of the region-wide geothermal gradient is ~20.1 ^{o}C km^{-1} which is the average of all measurements. This average gradient indicates that the groundwater temperature reaches 31.1 ^{o}C at about 1,000 m (assuming an average surface temperature of 11^{o}C; Fig. 12). If the basin-wide geothermal gradient is calculated using the 5 lowest gradients (16.2 ^{o}C km^{-1}; Table 2), 31.1 ^{o}C will be reached at about 1265 m depth (Fig. 12, and if the basin-wide geothermal gradient is calculated using the 5 highest gradients (24 ^{o}C km^{-1}; Table 2), 31.1 ^{o}C is reached at about 850 m depth (Fig. 12). These data indicate the Georgia Basin is a low geothermal gradient basin that is favourable for CO_2 sequestration and that CO_2 will reach a supercritical state between 850 m and 1,265 m depth.

UWI	Ground elevation (m)	Kelly bushing (KB) (m)	Depth of temperature measurement (m)	Wireline Log BHT (ºC)	DST temperature (ºC)	Geothermal gradient based on BHT (ºC)	Geothermal gradient based on DST (ºC)	Remarks
Canada								
D-007-A/092-G-03	55.1	60.5	1,440.1	50		27.1		-
			2,352.4	57		19.5		Temp measured 7 hours after circulation
			3,393.3	65		15.9		Temp measured 4 hours after circulation
			3,573.4–3,588		75		17.8	-
			4,369.9	77		15.1		Temp measured 6 hours after circulation
A-028-A/092-G-03	61.2	63.3	1,842.2	42		16.8		-
C-087-D/092-G-02/2	1.0	4.8	1,010−1,018.9		30		18.7	-
			1,270.0	38		21.3		-
D-095-D/092-G-02	0.5	4.6	670−681		27		23.6	-
			1,700.0	38		15.9		-
B-051-C/092-G-02	109.7	113.6	1,440.0	50		27.1		
			1,602.9	39		17.4		Temp measured 4 hours after circulation
			2,582.8	49		14.7		-
			3,319.8	65		16.2		Temp measured 7 hours after circulation
A-017-B/092-G-02	23.1	26.2	1,571.2	34		14.6		Temps measured 6 hours after circulation
A-097-A/092-G-02	85.2	91.5	928−939		37		27.8	-
			1,372−1,381		45		24.7	-
			2,626.3	52		15.6		-
D-003-A/092-G-02	50.0	56.3	2,116−2,117.7		58		22.2	-
			2,419.0	54		17.8		-
C-011-D/092-G-01	40.2	42.3	2,256.0	48		16.4		Temp measured 9 hours after circulation
			2,347.3−2,391.5		54		18.0	-
B-056-C/092-G-01	66.1	70.1	956.1	25		14.7		Temp measured 4 hours after circulation
D-077-E/092-H-04	10.9	13.1	1,559.9	51		26.4		Temp measured 7 hours after circulation
			1,885.7	61		26.5		-
USA								
5-39N-1E (W-72)	43.8	-	1,899.2	50		20.5		-
23-39N-1E (431)	73.4	78.9	1,823.0	44		18.1		-
26-39N-2E (432)	27.4	32.9	1,347.2	40		21.6		-
4-40N-3E (166)	37.1	40.2	1,847.0	52		22.2		-
			2,234.1	55		19.6		-
18-38N-4E (235)	163.9	167.0	1,683.4	53		25.0		-
13-39N-3E (456)	42.6	-	381.6	20		23.5		-
32-40N-1E (420)	23.4	27.4	1,966.2	47		18.3		-

UWI	Ground elevation (m)	Kelly bushing (KB) (m)	Depth of temperature measurement (m)	Wireline Log BHT (ºC)	DST temperature (ºC)	Geothermal gradient based on BHT (ºC)	Geothermal gradient based on DST (ºC)	Remarks
			1,966.2	57		23.3		-
			2,781.6	64		19.0		-
			2,781.3	82		25.5		-

Table 2 – Geothermal gradients calculated for 11 wells in the LMBC and 7 wells in northwest Washington State, USA, with bottom hole temperatures from wireline logs and DSTs. The average surface temperature used for calculating geothermal gradients is 11ºC (England, 1991).

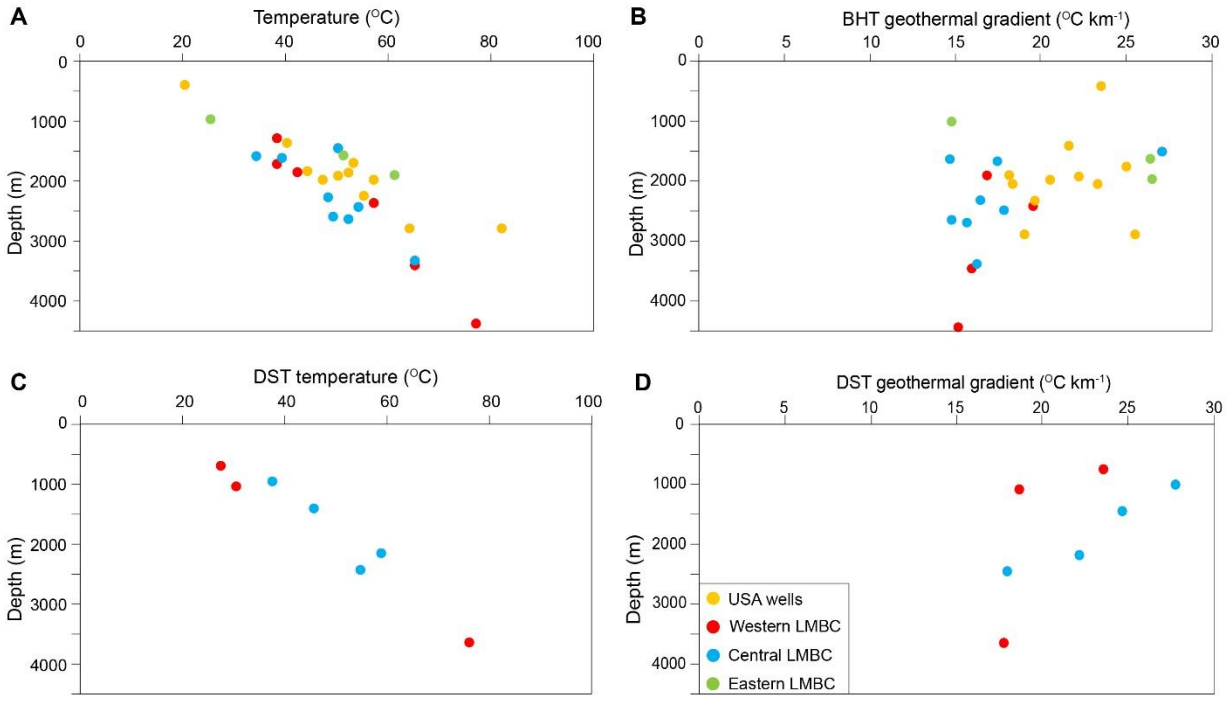

Figure 14 (two columns) – A) Bottom hole temperatures (BHT) from wireline logs versus depth for the 11 wells in the LMBC and 7 wells from Washington State, USA. B) Geothermal gradients calculated using BHT temperatures. C) Temperatures measured during DSTs. D) Geothermal gradients calculated using DST-based temperature measurements.

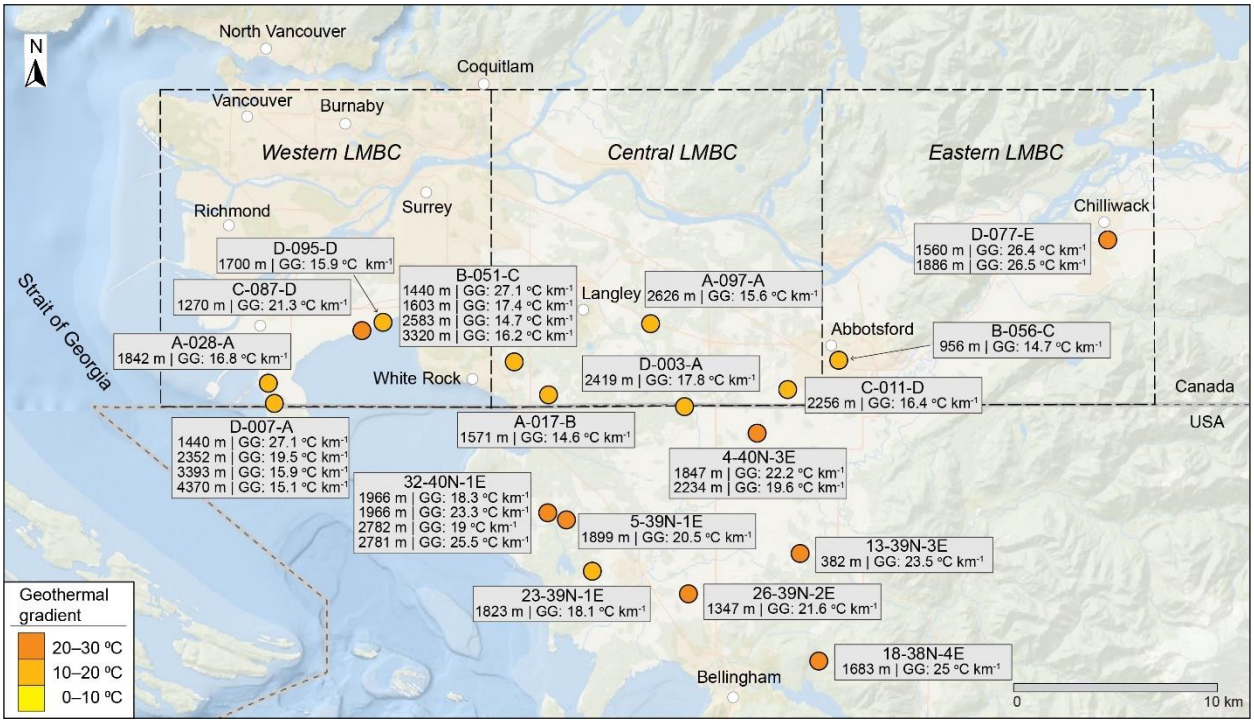

Figure 15 (two columns) – Geographical distribution of geothermal gradients calculated for wells with available bottom hole temperatures in the American and Canadian sectors of Georgia Basin.

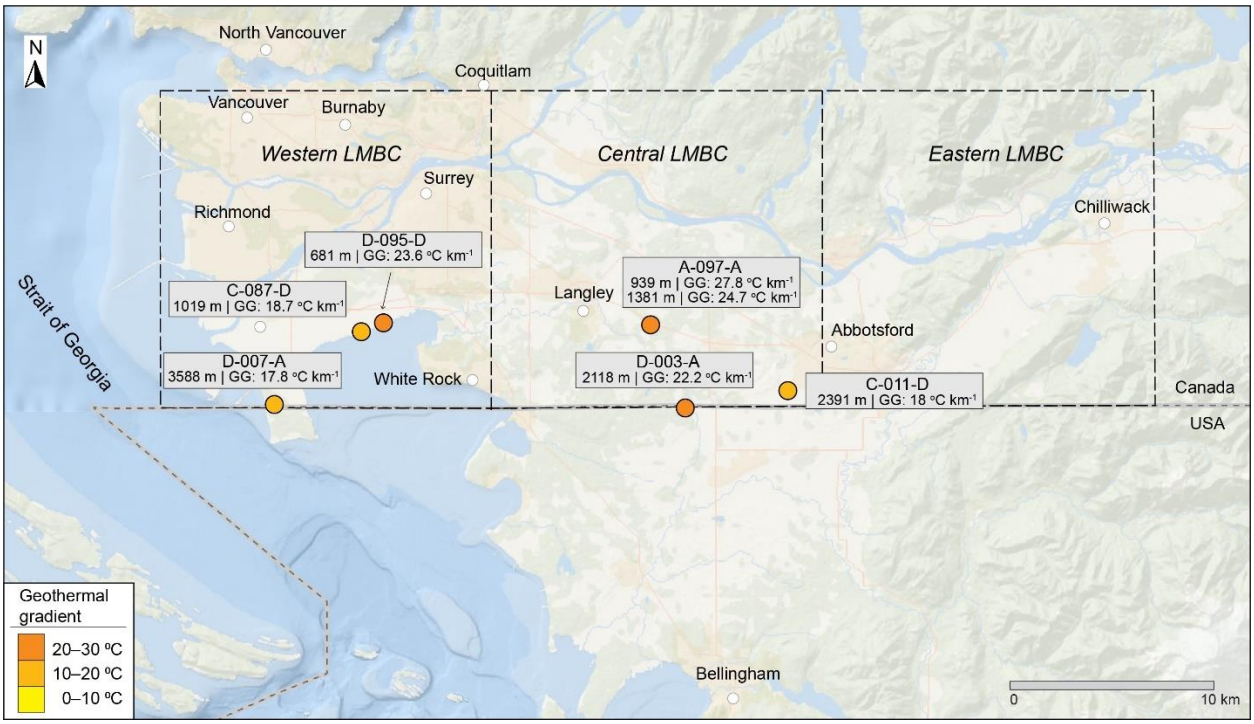

Figure 16 (two columns) – Geographical distribution of geothermal gradients calculated from DST-based temperatures.

4.2 Reservoir depth and thickness

A minimum saline aquifer thickness of 30 m is typically required to ensure sufficient reservoir volume for effective CO_2 storage (Metz et al., 2005). Reservoir thickness varies based on heterogeneity, reservoir geometry, porosity, permeability, and fluid properties, and hence, site-specific geological assessments and engineering considerations are pivotal to determining the minimum reservoir thickness for CO_2 storage in a particular location (Keighley and Maher, 2015).

The LMBC overlies >4,500 m of sedimentary strata in the southern extent of Western LMBC (i.e., Tsawwassen area, Fig. 2) and these strata thin to the north and east. Based on available well data, core, and geological reports, strata underlying the LMBC comprise mainly Tertiary and Upper Cretaceous strata (Table 3). Tertiary strata reach a maximum thickness of ~2,800 m (mainly in Western LMBC) and consist mostly of interbedded sandstone, mudstone, and coal (Fig 17; Sproule, 1976). Note that the stratigraphic tops listed in Table 3 and shown on Figure 17 are based on drilling reports, geological reports, and Sproule (1976). The top of Upper Cretaceous strata occurs at approximately 3,069 m in well D-007-A/092-G-03 in Western LMBC and at approximately 525 m in well B-056-C/092-G-01 in Eastern LMBC. The basement of the Georgia Basin was not intercepted in wells in Western and Central LMBC. In Eastern LMBC, the basement was intercepted at relatively shallow depths (Fig. 17).

UWI	KB (m)	Total Depth (m)	Top Tertiary (m)	Total Thickness of Tertiary (m)	Top Cretaceous (m)	Basement (m)	Data Source
Canada							
A-028-A/092-G-03	63.3	1,842.2	503.5	1,338.7+	NP	NP	Sproule (1976); well geological reports
D-007-A/092-G-03	60.5	4,508.6	252.8	2816.3	3,069.2	NP	
C-087-D/092-G-02/2	4.8	1,270.0	590.7	679.3+	NP	NP	
B-051-C/092-G-02	113.6	3,322.0	562.1	2184.3	2,746.4	NP	
A-017-B/092-G-02	26.2	1,585.6	475.5	1,110.1+	NP	NP	
A-097-A/092-G-02	91.5	2,635.0	253.5	2279.6	2,533.1	NP	
D-003-A/092-G-02	56.3	2,432.0	249.0	2127.9	2,376.9	NP	
C-011-D/092-G-01	42.3	2,396.3	312.4	1423.4	1,735.8	1,874.4	
B-056-C/092-G-01	70.1	958.0	NP	0	524.8	682.7	
D-077-E/092-H-04	13.1	1,885.8	NP	0	755.2	1,747.1	
USA							
23-39N-1E (431)	78.9	1,831.4	429.7	1,402.1+	NP	NP	well geological reports
13-39N-3E (456)	42.6	391.6	24.3	367.3+	NP	NP	
17-38N-4E (170)	214.2	1,434.6	243.8	1036.3	1,280.1	NP	
26-32N-2E (457)	27.4	560.8	79.2	481.5+	NP	NP	

Table 3 – Wells with stratigraphic tops for Tertiary and Upper Cretaceous strata and their thickness variations across the LMBC and northwest Washington State, USA. "+" in the total thickness of the Tertiary column indicates the thickness of the Tertiary strata exceeds the value listed as the base of the Tertiary was not intercepted. Note that tops for wells in the LMBC are largely derived from previously published reports, including drilling reports, geological reports, and Sproule (1976). Tops for wells in northwest Washington State are derived from the Washington Geologic Information Portal (2023). Acronyms: not present (NP).

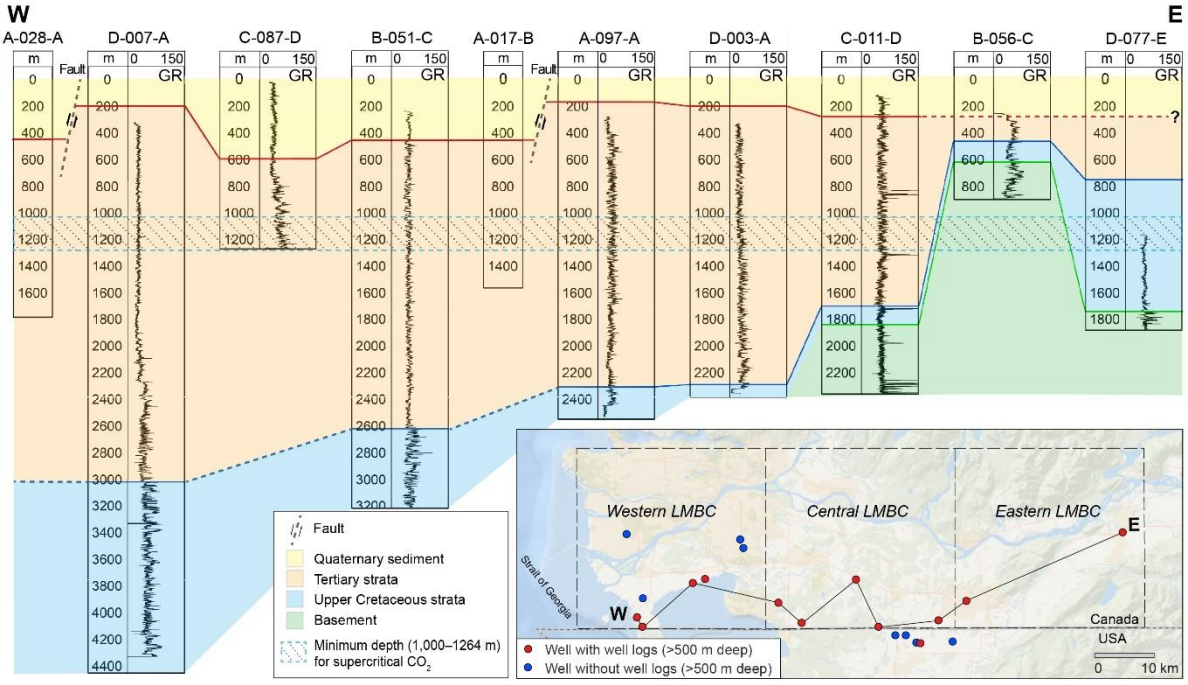

Figure 17 (two columns) – Structural cross-section across the LMBC. The datum is mean sea level. The depth columns are in true vertical depth relative to sea level (TVDSS). The light blue dashed line with stippled pattern indicates the predicted average depth of ~1,000 m for *ex-situ/in-situ* CO_2 dissolution and ~1,000–1,264 m for supercritical CO_2 storage. Stratigraphic tops are shown in Table 3.

4.3 Porosity and permeability

When supercritical/gaseous CO_2 or a CO_2-rich brine is injected into a reservoir, it replaces much of the resident pore fluid, and the effectiveness of a CO_2 sequestration project is determined largely by the storage volume and injectivity of the target reservoir. The storage volume available for supercritical/gaseous CO_2 or CO_2-rich brines varies as a function of effective porosity, area, thickness, and lithology of the reservoir as well as CO_2 solubility in water. The injection and subsequent migration of CO_2 /CO_2-rich brines are regulated by permeability (Doughty and Pruess, 2004; Miri and Hellevang, 2016; Worden, 2023). Reservoirs with the highest permeability enable increased and more efficient injection. Inadequate permeability, or baffles and barriers to fluid flow, such as faults or interbedded fine-grained layers, can lead to an increase in fluid pressure around the injection point, which limits the injection rate and, ultimately, the amount of CO_2 that can be injected (Bentham and Kirby, 2005). In low-permeability rocks, pressure gradients dissipate slowly, and fluid pressure gradually increases near the injection well. Typical reservoir porosity for CCS projects ranges from 5–30%, and permeability ranges from 20–3,500 mD (Bertier et al., 2006; Brennan and Burruss, 2006; Kuuskraa, 2004; Shafeen et al., 2004; Zweigel et al., 2004).

Below the LMBC, preserved Tertiary strata have net porous sandstone thicknesses of at least 447–1,256 m and average porosity derived from well-logs and using a 9% porosity cutoff ranges from ~12–23% (Table 4). In Upper Cretaceous strata well log coverage is incomplete, but where data is available, average porosity ranges from ~12.5–20%. At depths below 2,000 m, where primary matrix porosity is insignificant, secondary fracture porosity has been observed (Hannigan et al., 2001).

Core-derived porosity-permeability for Tertiary strata in well D-095-D/092-G-02 (943.5–957.5 m: 61 core plugs) is higher overall than in Tertiary strata at greater depth in well A-017-B/092-G-02 (1,298.6–1,389.4 m: 32 core plugs; Fig. 18). Mercury capillary pressure tests were performed on three core plugs (samples 17 (948.7 m), 44 (953.2 m), and 55 (955.5 m)) from well D-095-D/092-G-02 (Fig. 19A). The range of pore throat radius for the available samples varies from 0.05–12.2 µm (Fig. 19B). While the data are limited, they indicate that porosity and permeability decrease with depth and higher permeability correlates to larger pore throat sizes; both of these outcomes are expected in siliciclastic reservoirs. Available porosity and permeability data suggest that Tertiary strata underlying the LMBC have acceptable pore volume and injectivity capacity for CCS.

No core-derived porosity and permeability data are available for Upper Cretaceous strata at present. Based on the available well logs in Upper Cretaceous strata, net porous sandstone thicknesses is at least ~43.7–447 m and average porosity is ~12.5–20% (considering 9% porosity cutoff; Table 4).

UWI	Total Thickness (m)	Net porous sandstone @ 9% porosity cutoff (m)	Net: Gross Ratio (%)	Average porosity (%)	Remarks
Tertiary					
A-028-A/092-G-03	1,338.7	729.0	54%	12.0	Porosity calculated based on HMIN and HMNO
C-087-D/092-G-02	679.3+	447.0	65%	17.0	Porosity calculated based on GR and DEN logs
B-051-C/092-G-02	2,184.3	1,018.5	46%	19.0	Porosity calculated based on GR and SON logs
A-017-B/092-G-02	1,110.1	546.0	49%	23.0	Porosity calculated based on HMIN and HMNO
A-097-A/092-G-02	2279.6+	1,256.0	55%	15.0	Porosity calculated based on GR and SON logs
D-003-A/092-G-02	2127.9+	721.0	33%	17.0	Porosity calculated based on GR and SON logs
C-011-D/092-G-01	1,423.4	1,160.0	81%	17.5	Porosity calculated based on GR, HMIN, and HMNO
Upper Cretaceous					
B-051-C/092-G-02	575.6	128.0	22%	17.0	Porosity calculated based on GR and SON logs
A-097-A/092-G-02	101.9	68.0	66%	15.0	Porosity calculated based on GR and SON logs
D-003-A/092-G-02	55.1	43.7	79%	20.0	Porosity calculated based on GR and SON logs
C-011-D/092-G-01	138.6	86.0	62%	20.0	Porosity calculated based on GR, HMIN, and HMNO
B-056-C/092-G-01	158.0	75.0	47%	12.5	Porosity calculated based on GR and SON logs
D-077-E/092-H-04	992+	410.0	41%	17.0	Porosity calculated based on GR and SON logs

Table 4 – Well-log based average porosity and net porous sandstone thickness of Tertiary and Upper Cretaceous strata from 9 wells across the LMBC. A 9% porosity cutoff is considered for Tertiary and Upper Cretaceous strata. "+" indicates the minimum thickness because the well did not penetrate the full thickness of the interval. Remarks acronyms: Micro-Normal Resistivity (HMNO), Micro-Inverse Resistivity (HMIN), Gamma Ray (GR), Density (DEN), Sonic (SON).

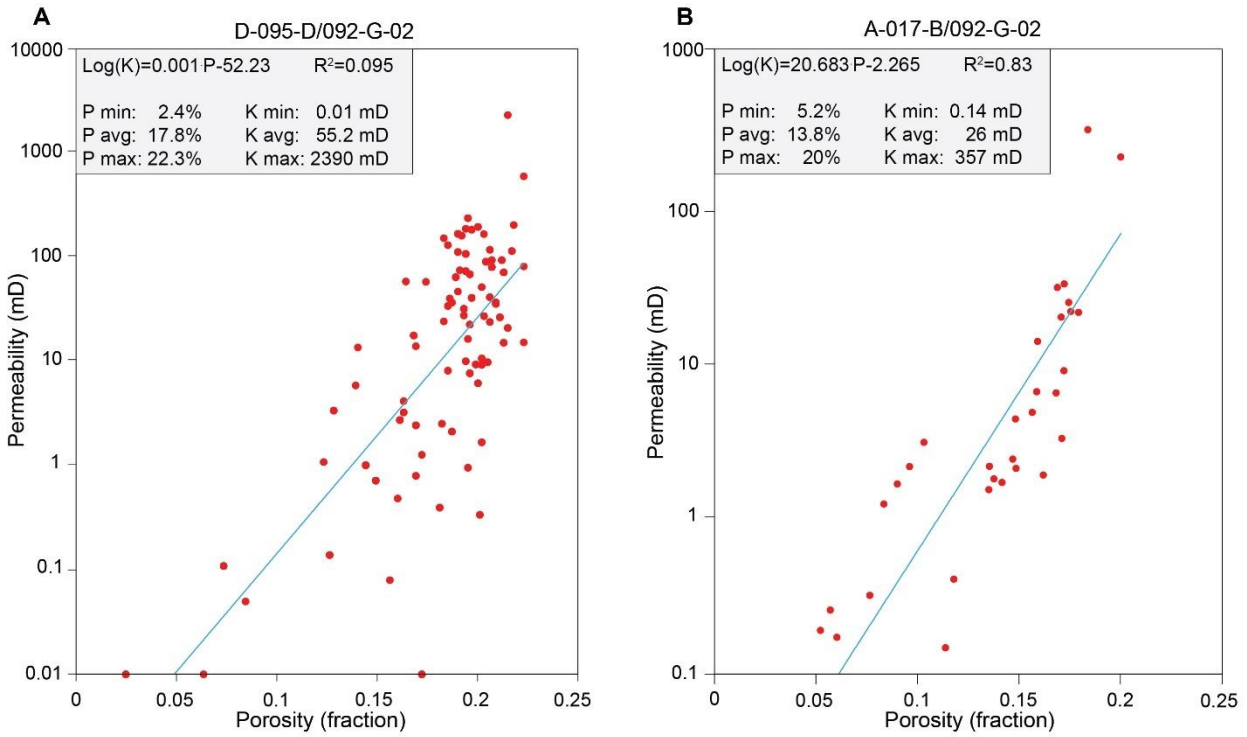

Figure 18 (one column) – Cross plots of core porosity versus core permeability for wells A) D-095-D/092-G-02, 943.5–957.5 m (61 core plugs), and B) A-017-B/092-G-02, 1,298.6–1,389.4 m (32 core plugs). Porosity was determined using Boyle's Law technique by measuring grain volume and bulk volume at ambient conditions. Permeability to air was measured on each sample using a steady-state method at minimum confining stress. Acronyms: porosity (P); permeability (K).

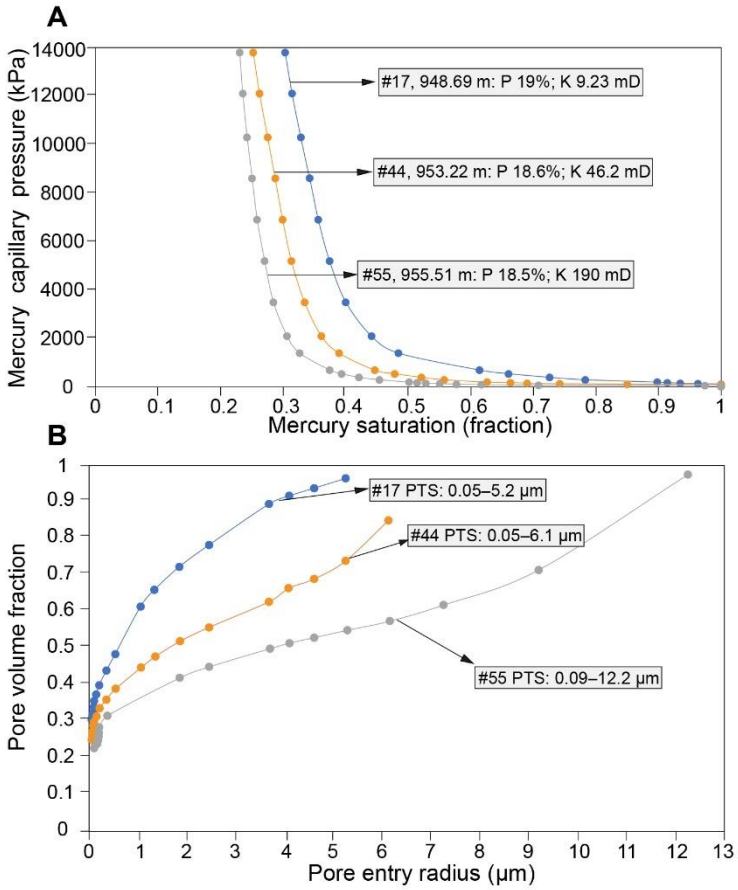

Figure 19 (one column) – A) Cross plot of mercury capillary pressure versus mercury saturation for 3 samples from well D-095-D/092-G-02. B) Pore entry radius versus pore volume function for the same 3 samples. Acronyms: porosity (P); permeability (K); pore throat size (PTS).

4.4 Porewater salinity

Salinity is the concentration of total dissolved solids (TDS in ppm), which includes a diverse range of substances such as minerals, salts, metals, and organic compounds. The cutoff value distinguishing between fresh and saline aquifers is typically based on the TDS content of the groundwater. Freshwater aquifers generally have a TDS concentration below a specific threshold, which is commonly set at ~1,000 ppm (Todd and Mays, 2004). Aquifers with TDS concentrations exceeding this threshold are categorized as saline aquifers. This threshold can, however, vary based on regional hydrogeological conditions and specific project requirements. The influence of salinity on the CO_2 storage capacity is significant as more CO_2 can be dissolved in freshwater than in saline water (Bachu, 2008). Additionally, salt precipitation near injection wells during CO_2 injection in saline aquifers may impair permeability and reduce injectivity (Zeidouni et al., 2009). High salinity (>100,000 ppm) can also lead to the formation of carbonates through

the reaction of CO_2 with minerals present in the water, particularly in areas close to injection wells; this reduces permeability and, ultimately CO_2 storage capacity (Bachu and Adams, 2003).

In LMBC, water samples collected from 7 wells provide limited information on the salinity of formation waters (Table 5). The TDS measurements for Tertiary strata exhibit considerable variation, ranging from 751–37,483 ppm, and these values depend on the type of test from which water samples were acquired and the timing of sampling relative to drilling. In some wells there are significant changes in measured values through time (e.g., C-011-D/092-G-01, Table 5) indicating that formation waters were contaminated with drilling mud; consequently, all salinity measurements are considered approximate. The highest TDS measured in Tertiary strata (37,483 ppm) is in Western LMBC. In Central LMBC, TDS values in Tertiary strata range from ~13,740 ppm in the Miocene Boundary Bay Fm to ~9,750 ppm in the Eocene Huntingdon Fm. The higher salinity in the Boundary Bay Fm compared to the Huntingdon Fm may be due to contamination during drilling, although more work is needed to confirm this. In Eastern LMBC, the salinity of water in Basement rock is predicted to be ~9,270 ppm, and in Upper Cretaceous strata, salinity is estimated at ~10,250 ppm. In Pleistocene strata in Western LMBC, salinity is ~2,200 ppm.

UWI	Test Type	Depth (m)	Strata/ Formation	Total dissolved solids (TDS) (ppm)	Probable TDS (ppm)	Density (g cm^{-3})	pH
Canada							
D-007-A/092-G-03	WS	2,188.5	Tertiary	37,483	**37,438**	1.033	10.3
B-051-C/092-G-02	DST 1	849.2-871.1	Miocene	13,741	**13,741**	1.014	7
	DST 4	1,468.2-1,479.2	Eocene	9,748	**9,748**	1.01	7.6
D-068-F/092-G-02	DST 4	1,107.9-1,158.8	Tertiary	751	**751**	-	-
C-011-D/092-G-01	WS-429P	2,362.2-2,366.8	Basement	5,965	**6,354**	1.003	7.8
	WS-430P			6,354		1.001	7.9
	WS-438P	2,366.8-2,377.4		9,268	**9,268**	1.005	6.8
	WS-436P	1,755.3-1,764.5	Upper Cretaceous	10,164	**10,248**	-	6.9
	WS-498P			5,266		1.001	7.1
	WS-499P			8,688		1.003	7.1
	WS-500P			9,619		1.004	6.9
	WS-501P			9,660		1.005	7.6
	WS-502P			9,959		-	7.1
	WS-503P			10,064		1.005	6.8
	WS - 504P			10,211		1.004	6.4
	WS-505P			10,554		1.004	6.7
	WS-506P			9,876		1.004	6.4
D-095-D/092-G-02	DST 1-a	670-681	Pleistocene	1,731	**2,198**	1.002	8
	DST 1-b			2,009		1	8
	DST 1-c			2,198		1	8

UWI	Test Type	Depth (m)	Strata/ Formation	Total dissolved solids (TDS) (ppm)	Probable TDS (ppm)	Density (g cm^{-3})	pH
A-017-B/092-G-02	DST 1-Test 3	732.1-739.1	Tertiary	2,481	**2,481**	-	7.7
	DST 2-Test 4	1,201.2-1,207		13,151	**13,151**	-	7.7
A-097-A/092-G-02	DST 1-Test 1	1,372-1,381	Tertiary	2,768	**2,768**	1	8.4
USA							
17-38N-4E (170)	?	949.4-958.5	Tertiary	40,000	**40,000**	-	-

Table 5 – Water analyses from 7 wells in LMBC. Abbreviations: drill stem test (DST), total dissolved solids (TDS), well swab (WS). The probable TDS is calculated using the average of the highest TDS values obtained from wells with multiple salinity measurements or by considering the highest TDS value recorded for wells with only one or two salinity measurements.

4.5 Mineralogy

The interaction of CO_2 with brine in aquifers can lead to changes in the reservoir's mineralogy, pH, isotopic composition, and ion concentration of the brine (Pearce et al., 2021). Siliciclastic saline reservoirs typically comprise sandstone with variable amounts of clay and silicate minerals. The reactivity of minerals in sandstone with CO_2 varies, with quartz and clay exhibiting low reactivity, while carbonate, plagioclase feldspar, and mafic minerals are more reactive. The reactivity of minerals in sandstone with CO_2 varies, with quartz and clay exhibiting low reactivity, while carbonate, plagioclase feldspar, and mafic minerals are more reactive (Gunter et al., 1997; Gunter et al., 1993; Kaszuba et al., 2003; Knauss et al., 2005; Rosenbauer and Thomas, 2010). In *ex-situ*/*in-situ* operations, injecting CO_2-rich brine into saline aquifers may cause the dissolution of feldspar and unstable minerals, leading to precipitation of quartz and/or calcite cement in pore spaces; these cements reduce injectivity (Ang et al., 2022). CO_2 injection in siliciclastic formations bearing carbonate minerals (e.g., calcium and magnesium) and mafic minerals (e.g., basalt-rich strata) can result in substantial sequestration through mineral trapping over hundreds to thousands of years (Amin et al., 2014; Bachu et al., 1994; Gunter et al., 1997; Gunter et al., 1993; Kaszuba et al., 2003, 2005; Knauss et al., 2005; Li et al., 2023; Moore et al., 2005; Xu et al., 2003, 2004).

In the LMBC, Tertiary strata comprise mainly quartz, detrital mica, chert, lithic fragments (including volcanic and metamorphic fragments), and feldspar (Gilley, 2003). Cements in Tertiary strata include calcite, silica, and clay, with calcite being the most prevalent (Gilley, 2003). Tertiary sandstones are classified as micaceous or carbonaceous. Feldspars and lithic fragments present in Tertiary sandstones are less degraded, have lower levels of silica cement, and exhibit less compaction when compared to Nanaimo Group sandstones (Gilley, 2003; Gordy, 1988; Hannigan et al., 2001). Sedimentary rocks of the Upper Cretaceous Nanaimo Group contain mainly quartz, feldspar, and rock fragments (chert, shale clasts, volcanic, plutonic, and metamorphic rock fragments etc.). Moreover, minor mica, glauconite, trace heavy metals, and organic matter are present. Typical cements in Nanaimo Group sandstones include calcite,

pyrite, potassium feldspar, plagioclase, clay minerals, and lesser dolomite (Van der Flier-Keller and Dumais, 1988; Zhai, 2015).

4.6 Reservoir pressure and confinement

The injectivity of CO_2 is influenced, in part, by the difference between reservoir pressure and bottom hole pressure, which impacts the efficiency and effectiveness of both supercritical/gaseous CO_2 and CO_2-rich brine injection operations (Ringrose, 2020; Worden, 2023). In most normally pressured reservoirs, the capacity to increase the bottom hole pressure is limited without compromising the caprock (Worden, 2023).

Pressure data obtained from DSTs provide information on various aspects of a reservoir, including its size, connectivity, permeability, pressure, formation damage, and potentially the type of fluid present. In the LMBC, DSTs were conducted in nine wells (over 19 intervals) and test Basement (3 intervals in 2 wells), Upper Cretaceous (2 intervals in 1 well), and Tertiary strata (14 intervals in 7 wells; Table 6) based on published formation tops. Notably, where the final shut-in pressure (FSIP) is >1% lower than the initial shut-in pressure (ISIP), the tested reservoir is probably of limited size and is not a suitable target for CO_2 sequestration.

The DST results from Tertiary strata in the LMBC also provide insights into the permeability and reservoir characteristics of tested zones (Table 6). DSTs were conducted on Tertiary sandstone intervals between 700–2,491 m depth, and test results indicate that in some wells and intervals, Tertiary strata have suitable permeability and potential reservoir size to enable CO_2 sequestration. The limited DST data available for Upper Cretaceous strata indicate that reservoir size and permeability are both limited. This suggests the Upper Cretaceous may not be a primary target for CCS (Table 6) although more data is required to test this assumption. In addition, while existing data provide a broad picture of reservoir characteristics, site- and zone-specific pressure data are needed to characterize a target interval properly.

UWI	Depth (m)	Strata/ Formation	IHSP (psi)	IFP (psi)	ISIP (psi)	FFP (psi)	FSIP (psi)	FHSP (psi)	% Change	Recovery	Permeability (K) | Formation Damage (FD)
D-007-A/092-G-03	2,312.5–2,491.1	Tertiary	4,461	230	4,066	506	3,201	4,461	-21.3	301.8 m mud cut salty water	Misrun?
	3,079.7–3,100.4	Upper Cretaceous	6,292	1,399	1,403	1,414	-	6,283	-100.0	36.6 m mud	-
	3,573.5–3,588.1		7,258	1,449	1,358	1,463	-	7,236	-100.0	18.3 m mud	K: Low
B-051-C/092-G-02	849.2–871.1	Tertiary	1,486	893	1,092	1,083	1,088	1,462	-0.3	638.6 m salty water and 82.3 m mud	K: High; FD: none
	1,419.5–1,432.6		2,542	46	448	58	154	2,542	-65.0	21.3 m mud	K: low; FD: none.
	1,468.2–1,479.2		2,595	50	2,051	59	1,780	2,595	-13.1	7.6 m brackish water and 7.6 m mud	K: low. FD: none.
	1,848.6–1,870		3,234	75	213	82	95	3,241	-55.8	9.1 m mud	K: low; FD: none
A-017-B/092-G-02	732.1–739.1	Tertiary	1,220	235	1,015	710	890	1,200	-12.3	551.7 m salty water	K: high
	1,201.2–1,207		1,970	210	1,580	470	1,360	1,990	-13.9	527.3 m salty water	K: average; FD: none
	1,393.5–1,400.6		2,360	190	1,790	190	1,470	2,280	-17.9	82.3 m sulphurous mud	K: low. FD: none
C-087-D/092-G-02	821–830	Tertiary	1,370	1,127	1,176	1,179	1,182	1,357	0.5	815 m mud cut water	K: high; FD: none.
	1,010–1,018.9		1,620	226	1,400	613	1,382	1,608	-1.2	775 m mud cut water	K: average; FD: none
A-097-A/092-G-02	928–939	Tertiary	1,518	397	1,222	994	1,219	1,545	-0.2	401 m fresh water	K: average
	1,372–1,381		2,242	24	1,931	80	1,883	2,251	-2.5	46 m mud	K: low; FD: none
D-003-A/092-G-02	2,116–2,117.7	Tertiary	3,911	3,432	-	3,573	-	3,926	-	3 m mud	Misrun?
C-011-D/092-G-01	2,354–2,369	Basement	4,227	66	-	66	-	4,127	-	27.4 m mud	Misrun?
	2,347.3–2,391.5		3,655	40	1,935	42	-	3,634	-100.0	21.3 m mud	K: low
D-095-D/092-G-02	670–681	Quaternary or Tertiary?	1,055	68	938	930	930	1,036	-0.9	288 m fresh water	K: average; FD: none
D-077-E/092-H-04	1,853.1–1,885.7	Basement?	3,078	-	2,676	-	2,676	3,018	0.0	457.2 m fresh water	FD: none
			3,052	-	2,663	-	2,650	3,011	-0.5		

Table 6 – DST analyses for Basement, Upper Cretaceous, and Tertiary strata in 9 wells in the LMBC. Abbreviations: initial hydrostatic pressure (IHSP), final hydrostatic pressure (FHSP), initial shut-in period (ISIP), final shut-in period (FSIP), initial flow period (IFP), final flow period (FFP). The percent change is the difference in reservoir pressure at the end of the ISIP and FSIP which is calculated based on ((FSIP - ISIP) / ISIP * 100).

4.7 Seismicity

Injecting supercritical/gaseous CO_2 or CO_2-rich brine into deep saline aquifers poses a risk of inducing seismicity if injected fluids cause over-pressurization (McGarr et al., 2002; Zoback and Gorelick, 2012). Increasing injection pressure can lead to higher injectivity but also increases mechanical stress and deformation, which potentially causes microseismicity, fault reactivation, development of new fractures, ground surface uplift, and earthquakes (Cappa and Rutqvist, 2011; Ferronato et al., 2010; Rutqvist et al., 2007). Even relatively small earthquakes (magnitude 3 or less) can pose a threat to the integrity of CO_2 storage projects (Zoback and Gorelick, 2012). Consequently, it is important to identify pre-existing faults

and avoid injecting supercritical/gaseous CO_2 or CO_2-rich brines near these structural elements. Offset distances of 5 and 10 km between injection wells and faults have been suggested for supercritical CO_2 injection operations (Birkholzer et al., 2012; Celia et al., 2015; Garnett et al., 2019; Oldenburg, 2012; Wolhuter et al., 2019; Zoback and Gorelick, 2012), although lower offset distances (e.g., 2.5 km) may be acceptable for CO_2-rich brine injection operations.

Elevated seismic activity occurs in basins located on or near active margins, whereas intracratonic basins typically exhibit less seismicity (Celia et al., 2015). Southwestern British Columbia and northwestern USA are regions with high seismic hazards due to their proximity to an active subduction zone (Fig. 20; Milne et al., 1978). The 1946 Vancouver Island earthquake, with a magnitude of 7.3, is the largest earthquake recorded in the region in the past 75 years; however, evidence of much larger earthquakes is preserved in historical records and is predicted from computer modelling (Zelt et al., 2001).

Earthquakes in SW BC fall into two main categories: 1) crustal earthquakes, with epicenters either in the upper 33 km of the continental crust or at the boundary between the continental crust and oceanic plate, and 2) subcrustal earthquakes, which occur in the subducting Juan de Fuca Plate at depths below ~33 km (Mosher et al., 2000; Zelt et al., 2001). Compressive stress subparallel to the continental margin, oriented NNW, triggers crustal earthquakes, while subcrustal earthquakes result from tensional stress regimes within the subducted plate (Mosher et al., 2000). The LMBC has experienced relatively few shallow earthquakes (<6 km depth) over the past 46 years compared to further south and east. The largest shallow quakes experienced in the region include a magnitude 4.9 earthquake in 1975 and a magnitude 4.6 earthquake beneath the Strait of Georgia, 30 km west of Vancouver, on June 24, 1997 (Mosher et al., 2000). The 1997 earthquake was shallow and was felt throughout the Greater Vancouver Area.

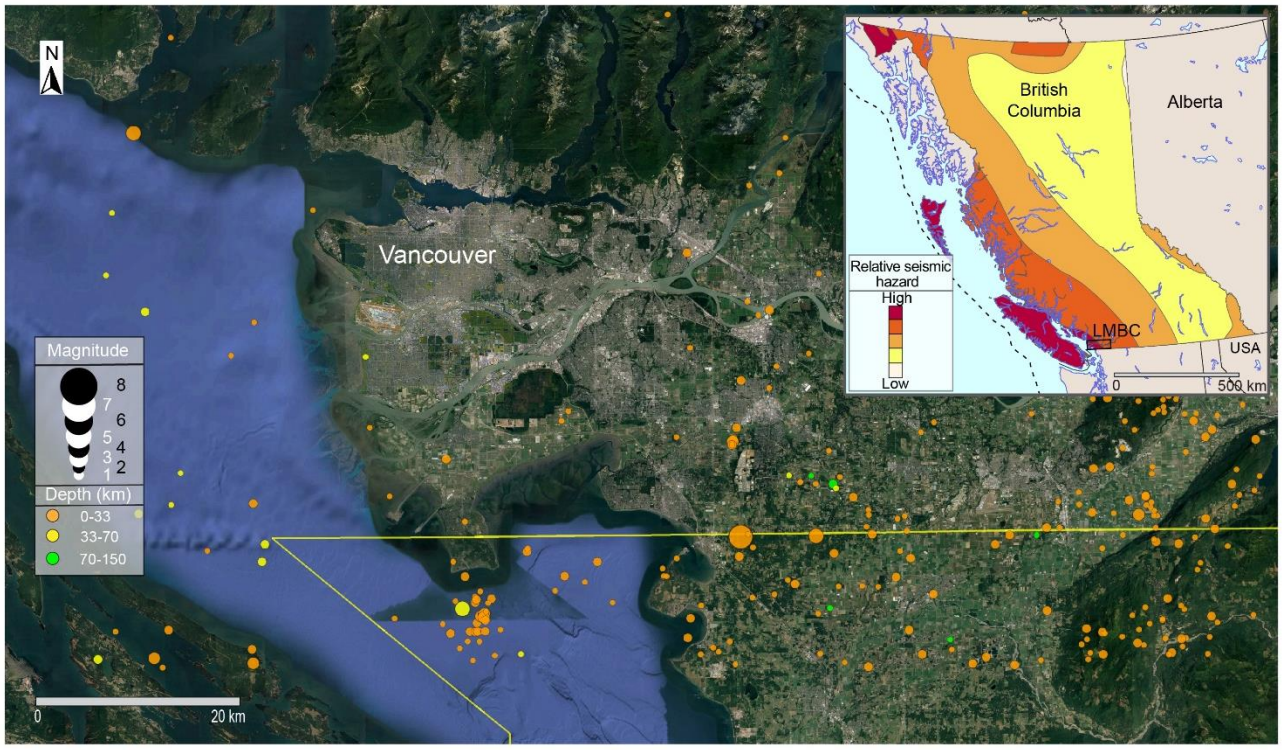

Figure 20 (two columns) – Earthquake map for southwest British Columbia and northwest USA. The inset map represents the relative seismic hazards in British Columbia (data derived from the United States Geological Survey, 2023). The black dashed line on the inset map marks the surface position of the subduction zone.

4.8 Faults

Sealed or partially sealed faults that crosscut potential CO_2 storage aquifers can compartmentalize the target reservoir, thereby increasing the overall complexity and cost of the storage project (Keighley and Maher, 2015). If some faults remain unsealed, they can significantly increase the risk of fluid leakage. Basins that have experienced multiple tectonic or deformation events are typically more heavily faulted and thus less suitable for CO_2 storage, especially for buoyant supercritical or gaseous CO_2 storage (Celia et al., 2015). Structural analysis is essential to assess the potential for leakage during the life cycle of a storage project (Keighley and Maher, 2015).

Two-dimensional seismic surveys acquired across the LMBC (Fig. 6) were used to map Upper Cretaceous and Tertiary surfaces and trace faults in the subsurface (Fig. 21). The surface maps of Upper Cretaceous and Tertiary strata were produced in studies in the 1970s evaluating underground gas storage potential in the LMBC (Hannigan et al., 2001) and Sproule (1976). Faults that crosscut Tertiary and Upper Cretaceous strata are dominantly normal or thrust faults. The number of faults and the vertical throw on those faults is greater in Upper Cretaceous strata compared to Tertiary strata. Some faults appear to extend through both

Upper Cretaceous and Tertiary strata. The distribution of faults that intersect both the Tertiary and Upper Cretaceous surfaces exhibits a variety of orientations, highlighting the complex nature of fault networks within the LMBC (Fig. 21). Faults that intersect the Upper Cretaceous surface are mainly normal faults with a dominant E–W orientation and secondary NE–SW orientation; thrust faults are dominantly NE–SW. Northeast–southwest-oriented normal faults dominate in Western LMBC, and E–W-oriented normal faults dominate in Central LMBC. Thrust faults within Upper Cretaceous strata occur mainly in Central LMBC. There are significantly fewer faults that intersect the top of Tertiary strata. These faults all appear to be connected to deeper seated faults (i.e., those that intersect the top of the Upper Cretaceous).

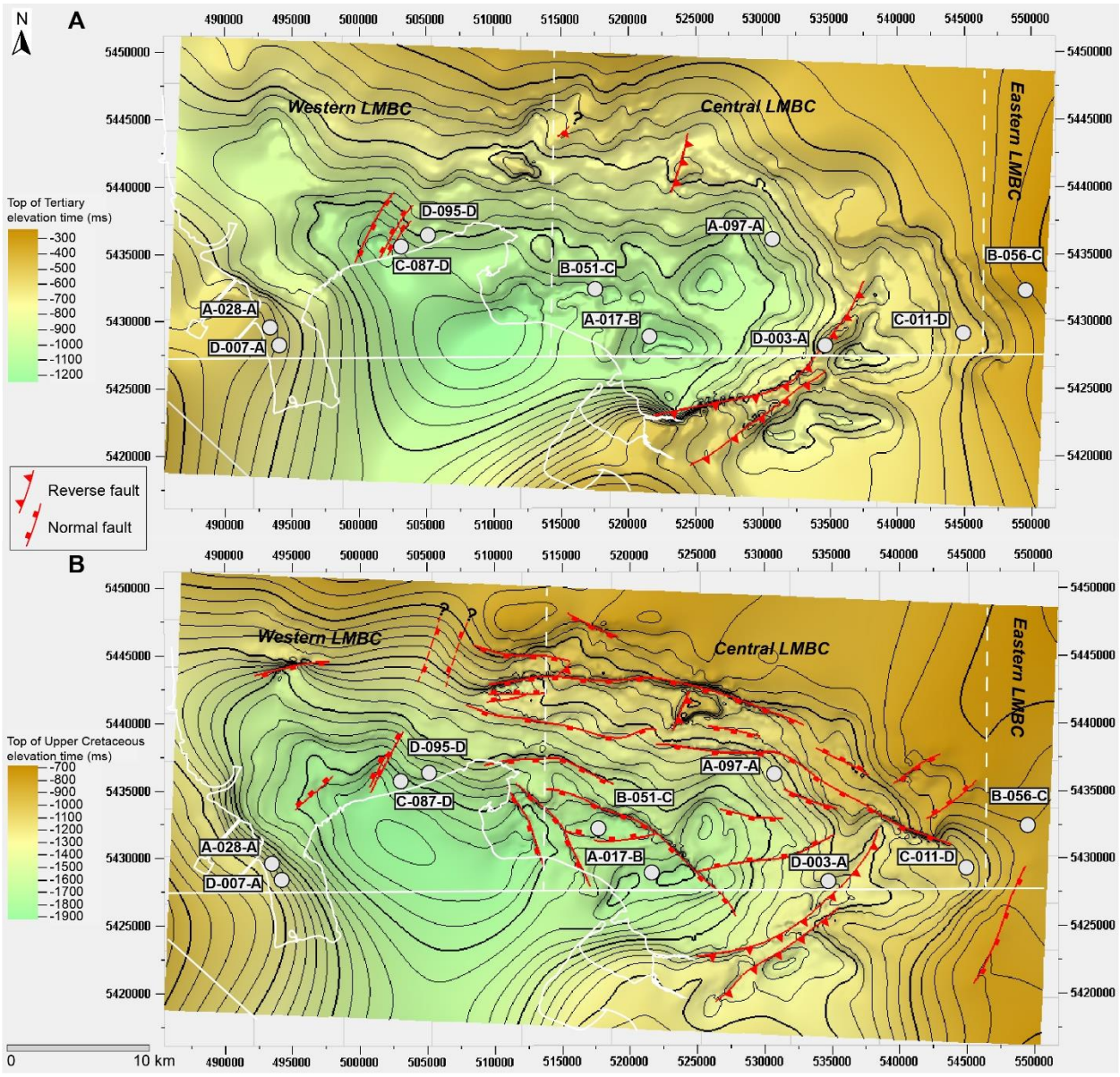

Figure 21 (two columns) – Fault traces (red lines) and types interpreted from 2D seismic data at the top of the A) Tertiary and B) Upper Cretaceous. The domain of both maps is time (data and fault interpretations are derived from Sproule (1976) and BC Gas (now FortisBC)).

5. Discussion

The primary risks associated with underground CO_2 storage in tectonically active regions are leakage of supercritical/gaseous CO_2 or CO_2-rich brine, ground deformation, and induced seismicity, and both natural and anthropogenic factors impact these risks. Natural factors include unidentified fractures or faults in the impermeable rock surrounding or overlying the injection zone, which can act as pathways for CO_2 leakage, and earthquakes that can initiate movement on active and unsealed/sealed faults. When

supercritical/gaseous CO_2 or CO_2-rich brine is injected at high pressure into underground reservoirs, it can increase stress in the reservoir. This increased stress leads to induced seismicity and the development and propagation of fractures when the hydrostatic pressure exceeds the lithostatic pressure of the reservoir and/or caprock. The presence of pre-existing faults or fractures can act as initiation points for induced seismicity particularly at high (above normal hydrostatic) reservoir pressures. The rate at which supercritical/gaseous CO_2 or CO_2-rich brine is injected and the total volume that is injected can impact pressure buildup in the reservoir. Anthropogenic factors include poorly sealed boreholes that penetrate a CO_2 injection site, and injecting CO_2 in an overpressured state and inducing fracturing, seismicity, and/or ground deformation.

The LMBC is in a tectonically active region, and it is generally not recommended to inject supercritical or gaseous CO_2 in such regions due to the risk of buoyant CO_2 leakage along new or existing faults. Given the apparent absence of regionally extensive and impermeable caprocks within Tertiary strata below the LMBC (Fig. 17) and the distribution of faults (Fig. 21), the risk of supercritical or gaseous CO_2 leakage into shallow aquifers and/or to surface is deemed to be high and so supercritical or gaseous CO_2 injection is not recommended at this time. *In-situ*/*ex-situ* schemes, where the density of a CO_2-rich brine exceeds that of the aquifer brine, significantly reduce the risk of CO_2 leakage as the CO_2-rich brine is negatively buoyant. In the LMBC, *in-situ/ex-situ* disposal of CO_2 is potentially possible in coal seams and deep saline aquifers, assuming reservoir conditions (temperature, pressure, injectivity, capacity, etc.) are suitable for sequestration. The targets for CO_2-rich brine storage (i.e., *in-situ/ex-situ* disposal) below the LMBC are Upper Cretaceous and Tertiary strata that possess favorable reservoir characteristics, are deeper than 1,000 m and are at least 5 km from mapped faults. Below, we discuss the potential of sequestering CO_2 in Upper Cretaceous and Tertiary strata below the LMBC.

5.1 CO_2 sequestration potential in Upper Cretaceous strata

The deepest potential reservoir target below the LMBC is the Upper Cretaceous Nanaimo Group. Upper Cretaceous strata below Western and Central LMBC occur at depths below ~3,070 m and ~1,735 m, respectively (Fig. 17), which is well below the minimum injection depth (1,000 m) for CO_2-rich brine storage. In Eastern LMBC, Upper Cretaceous strata are found at shallower depths (B-056-C/092-G-01 and D-077-E/092-H-04; Table 3) ranging from shallower than ~1,000 m (e.g., B-056-C/092-G-01) to ~1,700 m depth (e.g, D-077-E/092-H-04). In Eastern LMBC, only strata below 1,000 m have CO_2-rich brine injectivity potential.

Well-log-based porosity measurements for Upper Cretaceous strata range from ~12.5–20% (average:16.9% and using a 9% porosity cutoff; Table 4). In Western LMBC, porosity measurements and net porous sand thickness cannot be assessed accurately because either Upper Cretaceous strata are not encountered or available well logs do not enable porosity evaluation through the interval. In Central LMBC, net porous sandstone thickness ranges from at least ~43.7 m to 447 m and porosity ranges from ~15–20% (Table 4). In Eastern LMBC, net porous sandstone thickness ranges from at least 75 m to 410 m and porosity measurements range from ~12.5–17% (Table 4). Note that net porous sand thickness is derived from well logs that do not completely penetrate the Upper Cretaceous interval (Fig. 17; Table 3); consequently, net porous sand thicknesses are probably higher than the values reported here. There are no core-derived porosity or permeability data for Upper Cretaceous strata below the LMBC. A single DST from what is defined as Upper Cretaceous in Western LMBC (D-007-A/092-G-03, Table 6) indicates that reservoir size, continuity and permeability are all low in the tested interval.

In addition to reservoir quality, the number and extent of faults increase the probability of CO_2 leakage. Offset distances of 5 and 10 km have been proposed for supercritical/gaseous CO_2 injection (Birkholzer et al., 2012; Celia et al., 2015; Garnett et al., 2019; Oldenburg, 2012; Wolhuter et al., 2019; Zoback and Gorelick, 2012), while a smaller offset distance (2.5 km) may be possible for *in-situ/ex-situ* disposal operations. The density of faults in Upper Cretaceous strata appears to be lower in Western LMBC compared to Central and Eastern LMBC (Figs. 21B and 22), but this may be a manifestation of the limited seismic data in Western LMBC (Fig. 6). Using a 5 km minimum offset distance, most Upper Cretaceous strata in Central LMBC is situated close to a fault (Fig. 22); however, many of these faults only penetrate through the Upper Cretaceous interval and do not extend upwards through Tertiary strata (Fig. 21). In Western LMBC some areas are sufficiently offset from known faults (>5 km away), but the sparse seismic data in this region adds significant uncertainty. There is virtually no subsurface data available for Upper Cretaceous strata in Eastern LMBC.

The combination of extensive faulting and uncertainty regarding reservoir architecture and quality (due to very limited data) suggests that Upper Cretaceous strata below the LMBC should not be the primary target for CO_2 storage at present. Notably, however, given that only a few faults present in Upper Cretaceous strata extend upwards through all Tertiary strata (Fig. 21), the risk of leakage of CO_2-rich brine along faults may not be as significant where faults are contained to Upper Cretaceous strata only. Significantly more data and site-specific assessments are needed before the storage potential for CO_2 in Upper Cretaceous strata can be accurately assessed.

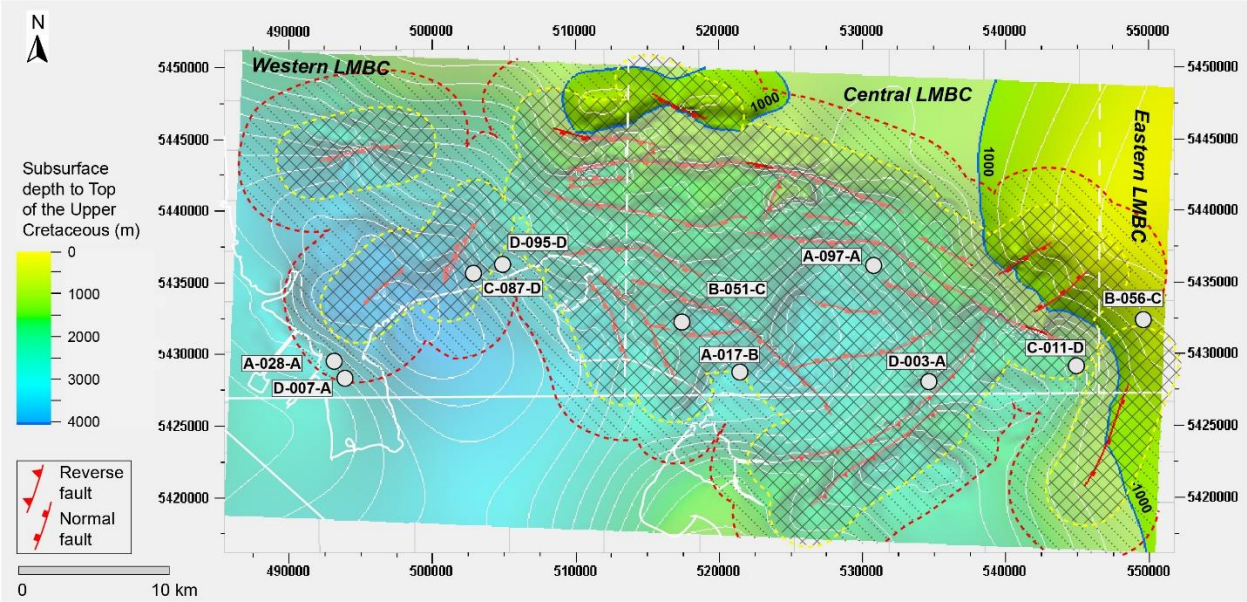

Figure 22 (two columns) – Map of the top of Upper Cretaceous strata below the LMBC. The 1,000 m contour line (blue) differentiates regions where Upper Cretaceous strata occur at depths suitable for CO_2-rich brine storage (without considering existing faults) and these areas are shaded. Dashed lines demarcate 2.5 km (yellow) and 5 km (red) offset distances from known faults. Cross-hatch and stippled patterns define regions that are within 2.5 km and 2.5 to 5 km of known faults, respectively.

5.2 CO_2 sequestration potential in Tertiary strata

Tertiary strata exhibit the greatest thickness among potential reservoir intervals (Table 3; Fig. 17; Sproule (1976)), and these strata become thin to the east and north. Tertiary strata below Western and Central LMBC occur at depths below ~252–590 m and ~250–562 m, respectively (Table 3; Fig. 17). In Eastern LMBC, Tertiary strata thin and reservoir data is limited, Tertiary strata consist primarily of sandstone, coal, and siltstone, and both sandstone intervals and coal seams are potential targets for *in-situ/ex-situ* CO_2 sequestration. In Western and Central LMBC, some Tertiary strata exhibit suitable characteristics for CO_2 sequestration, including good reservoir quality and size and suitable depth. Porosity measurements from well logs in Western LMBC range from ~12–18% (average: 15.6%) in Tertiary strata, and the average net porous sandstone thickness is ~750 m (Table 4). Porosity measurements from well logs in Central LMBC indicate even higher porosity in Tertiary strata (average: 18.3%) and an average of ~940 m of net porous sandstone (Table 4). Porosity and permeability measurements obtained from core samples in two wells (D-095-D/092-G-02 and A-017-B/092-G-02) in Western and Central LMBC indicate that Tertiary strata in these regions are potentially suitable for CO_2 storage (Fig. 18). Available data derived from DSTs reveal that some Tertiary strata in Western and Central LMBC exhibit good reservoir size and permeability (Table

6). Taken together, the data suggest that Tertiary strata in Western and Central LMBC possess sufficient storage and injectivity capacity for *in-situ/ex-situ* CO_2 sequestration.

In Eastern LMBC, core and DST data are insufficient to assess reservoir size and continuity, and Tertiary strata progressively thin and shallow towards the east. These data suggest that Tertiary strata are probably not prospective for CO_2 storage in Eastern LMBC, although site-specific assessments may reveal prospective areas and target horizons.

Fault density in Tertiary strata through Central and Western LMBC is low relative to the Upper Cretaceous, and the reduced number of faults minimizes the risk of long-term CO_2 leakage. Due to the absence of seismic coverage in Eastern LMBC, fault distributions are unknown. Where Tertiary strata exist below 1,000 m and at least 2.5 km from known faults, they are considered prospective for CO_2 storage, especially using *ex-situ* or *in-situ* sequestration (Fig. 23). The risk of CO_2 leakage decreases further if 5 and 10 km offset distances are used from known faults.

The risk associated with injecting into Tertiary strata is considerably lower than Upper Cretaceous strata, although data from both stratal intervals remains limited across the LMBC. Tertiary strata exhibit reasonable reservoir quality between 1,000 and 2,000 m depth in Western and Central LMBC; hence, we suggest these strata are the most suitable for CO_2 storage. Nonetheless, further investigation is needed to identify suitable horizons within Tertiary strata and Western and Central LMBC before site-specific assessments occur.

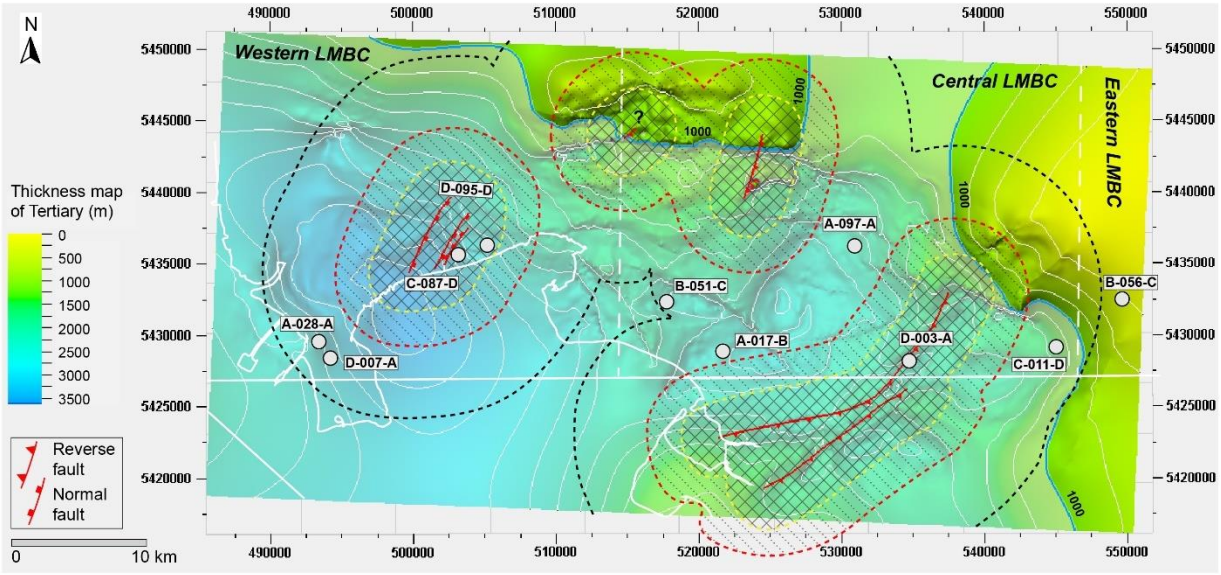

Figure 23 (two columns) – Thickness map of Tertiary strata below the LMBC. The 1,000 m depth contour line (blue) differentiates regions where Tertiary strata occur at depths suitable for CO_2-rich brine storage (without considering existing faults) and these areas are shaded. Dashed lines demarcate 2.5 km (yellow), 5 km (red), and 10 km (black) offset distances from known faults. Cross-hatch and stippled patterns define regions that are within 2.5 km and 2.5 to 5 km of known faults, respectively.

6. Conclusions

CCS is a promising and feasible solution for mitigating global CO_2 emissions while transitioning to a net-zero economy. Saline aquifers are key targets for CO_2 storage within subsurface geological formations; however, in areas with limited oil and gas production, the practicality and economic viability of underground storage is commonly assumed to be non-viable. Concerns around induced seismicity and fault-related CO_2 leakage must also be addressed in tectonically active regions.

Sedimentary strata below the LMBC comprise part of the fill of the Georgia Basin and include both Upper Cretaceous and Tertiary strata. Tertiary strata in Western and Central LMBC exhibit reservoir characteristics that are generally favorable for CO_2 storage, including suitable thickness, depth, reservoir quality, and limited faulting. *In-situ* or *ex-situ* CO_2 sequestration is probably more suitable than supercritical CO_2 sequestration. In Eastern LMBC, Tertiary strata thin and shallow and reservoir data is limited; consequently, Tertiary strata in Eastern LMBC should probably not be targeted for CO_2 storage at present.

Upper Cretaceous strata are encountered at depths of ~3,000 m in Western LMBC and ~2,400 m in Central LMBC. In both regions, Upper Cretaceous strata are intersected by numerous faults. There is also limited reservoir data for Upper Cretaceous strata and available data suggest reservoir storage potential (mainly porosity) may be good in Central LMBC. In Eastern LMBC, Upper Cretaceous strata occur at shallower depths and could potentially act as reservoirs for CO_2 storage but there is very little information on reservoir characteristics, stratal distribution, and faulting in Eastern LMBC. Overall, the prevalence of faults, greater depth, and uncertainty around reservoir characteristics of Upper Cretaceous strata suggest these rocks should not be the primary target for CO_2 without significantly more subsurface data.

This regional scale assessment of subsurface data in the LMBC provides a broad overview of the CO_2 storage potential in the region and demonstrate that there are areas (Western and Central LMBC) and intervals (Tertiary strata) in which CO_2 storage is possible especially for CO_2-rich brine. In Eastern LMBC, Upper Cretaceous strata are potentially prospective. Further refinement is needed to identify horizons within Tertiary strata (over 2,800 m thick in Western LMBC) that are most prospective for CO_2 storage.

7. Acknowledgements

The authors thank Nakari Diaz for assistance with generating several figures. We thank Jamilur Rahman, Warren Walsh whose advice and comments served to improve the quality of this manuscript. This study was funded through grants to S.E. Dashtgard from the BC Ministry of Energy, Mines, and Low-Carbon Innovation and the Natural Sciences and Engineering Research Council of Canada (RGPIN-2019-04528 and ALLRPP 581340-23).

8. References

Administration, N. O. a. A., 2022, Trend in atmospheric carbon dioxide.

Amin, S. M., Weiss, D., and Blunt, M., 2014, Reactive transport modelling of geologic CO2 sequestration in saline aquifers: The influence of pure CO2 and of mixtures of CO2 with CH4 on the sealing capacity of cap rock at 37 C and 100 bar: Chemical Geology, v. 367, p. 39-50.

Anderson, J., Bachu, S., Nimir, H. B., Basu, B., Bradshaw, J., Deguchi, G., Gale, J., von Goerne, G., Heidug, W., and Holloway, S., 2005, Underground geological storage, Cambridge University Press.

Ang, L., Yongming, L., Xi, C., Zhongyi, Z., and Yu, P., 2022, Review of CO2 sequestration mechanism in saline aquifers: Natural Gas Industry B.

Angus, S., Armstrong, B., and de Reuck, K., 1974, International Thermodynamic Tables of the Fluid State, Butterworths.

Bachu, S., 2000, Sequestration of CO2 in geological media: criteria and approach for site selection in response to climate change: Energy conversion and management, v. 41, no. 9, p. 953-970.

-, 2003, Screening and ranking of sedimentary basins for sequestration of CO2 in geological media in response to climate change: Environmental Geology, v. 44, no. 3, p. 277-289.

-, 2008, CO2 storage in geological media: Role, means, status and barriers to deployment: Progress in energy and combustion science, v. 34, no. 2, p. 254-273.

-, 2015, Review of CO2 storage efficiency in deep saline aquifers: International Journal of Greenhouse Gas Control, v. 40, p. 188-202.

Bachu, S., and Adams, J. J., 2003, Sequestration of CO2 in geological media in response to climate change: capacity of deep saline aquifers to sequester CO2 in solution: Energy Conversion and management, v. 44, no. 20, p. 3151-3175.

Bachu, S., Gunter, W., and Perkins, E., 1994, Aquifer disposal of CO2: hydrodynamic and mineral trapping: Energy Conversion and management, v. 35, no. 4, p. 269-279.

Bachu, S., and Gunter, W. D., 2005, Overview of acid-gas injection operations in western Canada, Greenhouse Gas Control Technologies 7, Elsevier, p. 443-448.

Bain, H. A., and Hubbard, S. M., 2016, Stratigraphic evolution of a long-lived submarine channel system in the Late Cretaceous Nanaimo Group, British Columbia, Canada: Sedimentary Geology, v. 337, p. 113-132.

Benson, S. M., and Cole, D. R., 2008, CO2 sequestration in deep sedimentary formations: Elements, v. 4, no. 5, p. 325-331.

Bentham, M., and Kirby, M., 2005, CO2 storage in saline aquifers: Oil & gas science and technology, v. 60, no. 3, p. 559-567.

Bertier, P., Swennen, R., Laenen, B., Lagrou, D., and Dreesen, R., 2006, Experimental identification of CO2–water–rock interactions caused by sequestration of CO2 in Westphalian and Buntsandstein sandstones of the Campine Basin (NE-Belgium): Journal of Geochemical Exploration, v. 89, no. 1-3, p. 10-14.

Birkholzer, J. T., Cihan, A., and Zhou, Q., 2012, Impact-driven pressure management via targeted brine extraction—Conceptual studies of CO2 storage in saline formations: International Journal of Greenhouse Gas Control, v. 7, p. 168-180.

Bradshaw, B. E., Spencer, L. K., Lahtinen, A.-L., Khider, K., Ryan, D. J., Colwell, J. B., Chirinos, A., Bradshaw, J., Draper, J. J., and Hodgkinson, J., 2011, An assessment of Queensland's CO2 geological storage prospectivity—The Queensland CO2 geological storage atlas: Energy Procedia, v. 4, p. 4583-4590.

Bratu, A., Card, K. G., Closson, K., Aran, N., Marshall, C., Clayton, S., Gislason, M. K., Samji, H., Martin, G., and Lem, M., 2022, The 2021 Western North American heat dome increased climate change

anxiety among British Columbians: Results from a natural experiment: The Journal of Climate Change and Health, v. 6, p. 100116.

Brennan, S. T., and Burruss, R. C., 2006, Specific storage volumes: A useful tool for CO 2 storage capacity assessment: Natural Resources Research, v. 15, p. 165-182.

Burruss, R. C., Brennan, S. T., Freeman, P. A., Merrill, M. D., Ruppert, L. F., Becker, M. F., Herkelrath, W. N., Kharaka, Y. K., Neuzil, C. E., and Swanson, S. M., 2009, Development of a probabilistic assessment methodology for evaluation of carbon dioxide storage: US Geological Survey Open-File Report, v. 1035, no. 2009, p. 81.

Burton, M., and Bryant, S. L., 2009, Surface dissolution: minimizing groundwater impact and leakage risk simultaneously: Energy Procedia, v. 1, no. 1, p. 3707-3714.

Bustin, R., 1995, Organic maturation and petroleum source rock potential of Tofino Basin, southwestern British Columbia: Bulletin of Canadian Petroleum Geology, v. 43, no. 2, p. 177-186.

Bustin, R., and England, T., 1991, P et roleum source rock potential of the Nanaimo G roup, western margin of the Georgia basin, southwestern British Columbia: Current Research, Part A, Geological Survey of Canada, p. 143.

Butler, V. L., Bovy, K. M., Campbell, S. K., Etnier, M. A., and Sterling, S. L., 2019, The Číxwicən project of Northwest Washington State, USA: opportunity lost, opportunity found: Journal of Archaeological Science: Reports, v. 23, p. 1095-1103.

Cao, F., Eskin, D., and Leonenko, Y., 2020, Modeling of ex-situ dissolution for geologic sequestration of carbon dioxide in aquifers: Journal of Petroleum Science and Engineering, v. 187, p. 106835.

Cappa, F., and Rutqvist, J., 2011, Impact of CO2 geological sequestration on the nucleation of earthquakes: Geophysical Research Letters, v. 38, no. 17.

Celia, M. A., Bachu, S., Nordbotten, J. M., and Bandilla, K. W., 2015, Status of CO2 storage in deep saline aquifers with emphasis on modeling approaches and practical simulations: Water Resources Research, v. 51, no. 9, p. 6846-6892.

Chiodini, G., Frondini, F., Cardellini, C., Granieri, D., Marini, L., and Ventura, G., 2001, CO2 degassing and energy release at Solfatara volcano, Campi Flegrei, Italy: Journal of Geophysical Research: Solid Earth, v. 106, no. B8, p. 16213-16221.

De Silva, G., Ranjith, P. G., and Perera, M., 2015, Geochemical aspects of CO2 sequestration in deep saline aquifers: A review: Fuel, v. 155, p. 128-143.

Doughty, C., and Pruess, K., 2004, Modeling supercritical carbon dioxide injection in heterogeneous porous media: Vadose Zone Journal, v. 3, no. 3, p. 837-847.

EIA, 2021, International Energy Outlook 2021: US Department of Energy, Washington, DC, 2021.

Eke, P. E., Naylor, M., Haszeldine, S., and Curtis, A., 2011, CO2/brine surface dissolution and injection: CO2 storage enhancement: SPE Projects, Facilities & Construction, v. 6, no. 01, p. 41-53.

Emami-Meybodi, H., Hassanzadeh, H., Green, C. P., and Ennis-King, J., 2015, Convective dissolution of CO2 in saline aquifers: Progress in modeling and experiments: International Journal of Greenhouse Gas Control, v. 40, p. 238-266.

England, T., 1991, Late Cretaceous to Paleogene structural and stratigraphic evolution of Georgia Basin, southwestern British Columbia: implications for hydrocarbon potential: Washington Geology, v. 19, no. 4, p. 10-11.

England, T., and Bustin, R., 1998, Architecture of the Georgia Basin southwestern British Columbia: Bulletin of Canadian Petroleum Geology, v. 46, no. 2, p. 288-320.

England, T., and Hiscott, R., 1992, Lithostratigraphy and deep-water setting of the upper Nanaimo Group (Upper Cretaceous), outer Gulf Islands of southwestern British Columbia: Canadian Journal of Earth Sciences, v. 29, no. 3, p. 574-595.

Englert, R. G., Hubbard, S. M., Coutts, D. S., and Matthews, W. A., 2018, Tectonically controlled initiation of contemporaneous deep-water channel systems along a Late Cretaceous continental margin, western British Columbia, Canada: Sedimentology, v. 65, no. 7, p. 2404-2438.

Ennis-King, J., Preston, I., and Paterson, L., 2005, Onset of convection in anisotropic porous media subject to a rapid change in boundary conditions: Physics of Fluids, v. 17, no. 8, p. 084107.

Ferronato, M., Gambolati, G., Janna, C., and Teatini, P., 2010, Geomechanical issues of anthropogenic CO2 sequestration in exploited gas fields: Energy Conversion and Management, v. 51, no. 10, p. 1918-1928.

Flannigan, M., and Wagner, C. V., 1991, Climate change and wildfire in Canada: Canadian Journal of Forest Research, v. 21, no. 1, p. 66-72.

Friedlingstein, P., O'sullivan, M., Jones, M. W., Andrew, R. M., Gregor, L., Hauck, J., Le Quéré, C., Luijkx, I. T., Olsen, A., and Peters, G. P., 2022, Global carbon budget 2022: Earth System Science Data Discussions, v. 2022, p. 1-159.

Friedlingstein, P., O'sullivan, M., Jones, M. W., Andrew, R. M., Hauck, J., Olsen, A., Peters, G. P., Peters, W., Pongratz, J., and Sitch, S., 2020, Global carbon budget 2020: Earth System Science Data, v. 12, no. 4, p. 3269-3340.

Garnett, A., Underschultz, J., and Ashworth, P., 2019, Scoping study for material carbon abatement via carbon capture and storage: Extended socio-economic-technical summary.

Gentzis, T., 2000, Subsurface sequestration of carbon dioxide—an overview from an Alberta (Canada) perspective: International Journal of Coal Geology, v. 43, no. 1-4, p. 287-305.

Gilley, B. H. T., 2003, Facies Architecture and Stratigraphy of the Paleogene Huntingdon Formation at Abbotsford, British Columbia.

Girotto, K., 2022, Tectono-stratigraphic model for the early evolution of the Late Cretaceous Nanaimo Group: Georgia Basin, British Columbia, Canada.

Gordy, P. L., 1988, Evaluation of the hydrocarbon potential of the Georgia depression: BC Ministry of Energy, Mines and Low Carbon Innovation.

Granieri, D., Chiodini, G., Marzocchi, W., and Avino, R., 2003, Continuous monitoring of CO2 soil diffuse degassing at Phlegraean Fields (Italy): influence of environmental and volcanic parameters: Earth and Planetary Science Letters, v. 212, no. 1-2, p. 167-179.

Gunter, W., Wiwehar, B., and Perkins, E., 1997, Aquifer disposal of CO2-rich greenhouse gases: extension of the time scale of experiment for CO2-sequestering reactions by geochemical modelling: Mineralogy and petrology, v. 59, no. 1-2, p. 121.

Gunter, W. D., Perkins, E. H., and McCann, T. J., 1993, Aquifer disposal of CO2-rich gases: reaction design for added capacity: Energy Conversion and management, v. 34, no. 9-11, p. 941-948.

Haggart, J. W., 1992, Progress in Jurassic and Cretaceous stratigraphy, Queen Charlotte Islands, British Columbia: Current research, part A. Geological Survey of Canada, Paper, v. 92, p. 361-365.

-, 1993, Latest Jurassic and Cretaceous paleogeography of the northern Insular belt, British Columbia.

Hannigan, P., Dietrich, J., Osadetz, K., and Lee, P., 2001, Petroleum resource potential of sedimentary basins on the Pacific margin of Canada, Geological Survey of Canada.

Hassanzadeh, H., Pooladi-Darvish, M., and Keith, D., 2005, Modelling of convective mixing in CO2 storage: Journal of Canadian Petroleum Technology, v. 44, no. 10.

Hassanzadeh, H., Pooladi-Darvish, M., and Keith, D. W., 2009, Accelerating CO2 dissolution in saline aquifers for geological storage・ Mechanistic and sensitivity studies: Energy & Fuels, v. 23, no. 6, p. 3328-3336.

Hassanzadeh, H., Pooladi-Darvish, M., and Keith, D. W., 2007, Scaling behavior of convective mixing, with application to geological storage of CO2: AIChE journal, v. 53, no. 5, p. 1121-1131.

Haywood, A. M., Dowsett, H. J., Dolan, A. M., Rowley, D., Abe-Ouchi, A., Otto-Bliesner, B., Chandler, M. A., Hunter, S. J., Lunt, D. J., and Pound, M., 2016, The Pliocene model intercomparison project

(PlioMIP) phase 2: scientific objectives and experimental design: Climate of the Past, v. 12, no. 3, p. 663-675.
Herzog, H., 2001, What future for carbon capture and sequestration?: Environmental Science and Technology-Columbus, v. 35, no. 7, p. 148A.
Hileman, B., 1997, Industry Considers CO2 Reduction Methods: Chemical & engineering news, v. 75, no. 26, p. 30-30.
Hitchon, B., 1996, Aquifer disposal of carbon dioxide: hydrodynamic and mineral trapping-proof of concept.
Holloway, S., and Savage, D., 1993, The potential for aquifer disposal of carbon dioxide in the UK: Energy Conversion and Management, v. 34, no. 9-11, p. 925-932.
Holtz, M. H., 2002, Optimization of CO2 Sequestered as a Residual Phase in Brine-Saturated Formations.
Hopkins Jr, W. S., 1968, Subsurface Miocene rocks, British Columbia-Washington, a palynological investigation: Geological Society of America Bulletin, v. 79, no. 6, p. 763-768.
Hopkins, W. S., 1966, Palynology of Tertiary rocks of the Whatcom Basin, Southwestern British Columbia and Northwestern Washington: University of British Columbia.
Huang, C., Dashtgard, S. E., Haggart, J. W., and Girotto, K., 2022, Synthesis of chronostratigraphic data and methods in the Georgia Basin, Canada, with implications for convergent-margin basin chronology: Earth-Science Reviews, v. 231, p. 104076.
Huang, C., Dashtgard, S. E., Kent, B. A., Gibson, H. D., and Matthews, W. A., 2019, Resolving the architecture and early evolution of a forearc basin (Georgia Basin, Canada) using detrital zircon: Scientific Reports, v. 9, no. 1, p. 15360.
IEA, 2021, Global Energy Review: CO2 Emissions in 2021—Analysis.
Iglauer, S., 2018, Optimum storage depths for structural CO2 trapping: International Journal of Greenhouse Gas Control, v. 77, p. 82-87.
Ismail, I., and Gaganis, V., 2023, Carbon Capture, Utilization, and Storage in Saline Aquifers: Subsurface Policies, Development Plans, Well Control Strategies and Optimization Approaches—A Review: Clean Technologies, v. 5, no. 2, p. 609-637.
Jafari, M., Cao, S. C., and Jung, J., 2017, Geological CO2 sequestration in saline aquifers: Implication on potential solutions of China's power sector: Resources, Conservation and Recycling, v. 121, p. 137-155.
Jenkins, C. R., Cook, P. J., Ennis-King, J., Undershultz, J., Boreham, C., Dance, T., De Caritat, P., Etheridge, D. M., Freifeld, B. M., and Hortle, A., 2012, Safe storage and effective monitoring of CO2 in depleted gas fields: Proceedings of the National Academy of Sciences, v. 109, no. 2, p. E35-E41.
Johnson, S., 1991, Sedimentation and tectonic setting of the Chuckanut Formation, northwest Washington: Washington Geology, v. 19, no. 4, p. 12-13.
Johnson, S. Y., 1984, Stratigraphy, age, and paleogeography of the Eocene Chuckanut Formation, northwest Washington: Canadian Journal of Earth Sciences, v. 21, no. 1, p. 92-106.
-, 1985, Eocene strike-slip faulting and nonmarine basin formation in Washington.
Johnston, W., 1923, Geology of Fraser River delta map-area: Geological Survey of Canada: Memoir, v. 135, p. 87.
Juanes, R., Spiteri, E., Orr Jr, F., and Blunt, M., 2006, Impact of relative permeability hysteresis on geological CO2 storage: Water resources research, v. 42, no. 12.
Kaszuba, J. P., Janecky, D. R., and Snow, M. G., 2003, Carbon dioxide reaction processes in a model brine aquifer at 200 C and 200 bars: implications for geologic sequestration of carbon: Applied geochemistry, v. 18, no. 7, p. 1065-1080.
-, 2005, Experimental evaluation of mixed fluid reactions between supercritical carbon dioxide and NaCl brine: Relevance to the integrity of a geologic carbon repository: Chemical Geology, v. 217, no. 3-4, p. 277-293.

Keighley, D., and Maher, C., 2015, A preliminary assessment of carbon storage suitability in deep underground geological formations of New Brunswick, Canada: Atlantic Geology, v. 51, p. 269-286.

Keith, D. W., Hassanzadeh, H., and Pooladi-Darvish, M., 2005, Reservoir engineering to accelerate dissolution of stored CO2 in brines, Greenhouse Gas Control Technologies 7, Elsevier, p. 2163-2167.

Kent, B. A., Dashtgard, S. E., Huang, C., MacEachern, J. A., Gibson, H. D., and Cathyl-Huhn, G., 2020, Initiation and early evolution of a forearc basin: Georgia Basin, Canada: Basin Research, v. 32, no. 1, p. 163-185.

Kharaka, Y. K., Cole, D. R., Hovorka, S. D., Gunter, W., Knauss, K. G., and Freifeld, B., 2006, Gas-water-rock interactions in Frio Formation following CO2 injection: Implications for the storage of greenhouse gases in sedimentary basins: Geology, v. 34, no. 7, p. 577-580.

Knauss, K. G., Johnson, J. W., and Steefel, C. I., 2005, Evaluation of the impact of CO2, co-contaminant gas, aqueous fluid and reservoir rock interactions on the geologic sequestration of CO2: Chemical geology, v. 217, no. 3-4, p. 339-350.

Kumar, A., Ozah, R., Noh, M., Pope, G. A., Bryant, S., Sepehrnoori, K., and Lake, L. W., 2005, Reservoir simulation of CO2 storage in deep saline aquifers: Spe Journal, v. 10, no. 03, p. 336-348.

Kumar, S., Foroozesh, J., Edlmann, K., Rezk, M. G., and Lim, C. Y., 2020, A comprehensive review of value-added CO2 sequestration in subsurface saline aquifers: Journal of Natural Gas Science and Engineering, v. 81, p. 103437.

Kuuskraa, V. A., Estimating CO2 Storage Capacity in Saline Aquifers, *in* Proceedings 3rd Annual Conference on Carbon Capture and Sequestration, Alexandria, Virginia2004, p. 3-6.

La Croix, A. D., Harfoush, A., Rodger, I., Gonzalez, S., Undershultz, J. R., Hayes, P., and Garnett, A., 2020, Reservoir modelling notional CO2 injection into the Precipice Sandstone and Evergreen Formation in the Surat Basin, Australia: Petroleum Geoscience, v. 26, no. 1, p. 127-140.

Lane, J., Greig, C., and Garnett, A., 2021, Uncertain storage prospects create a conundrum for carbon capture and storage ambitions: Nature Climate Change, v. 11, no. 11, p. 925-936.

Leonenko, Y., and Keith, D. W., 2008, Reservoir engineering to accelerate the dissolution of CO2 stored in aquifers: Environmental science & technology, v. 42, no. 8, p. 2742-2747.

Li, Z., Lv, Y., Liu, B., and Fu, X., 2023, Reactive Transport Modeling of CO2-Brine–Rock Interaction on Long-Term CO2 Sequestration in Shihezi Formation: Energies, v. 16, no. 2, p. 670.

Lynch, G., 1992, Deformation of Early Cretaceous volcanic-arc assemblages, southern Coast belt, British Columbia: Canadian Journal of Earth Sciences, v. 29, no. 12, p. 2706-2721.

Lynch, J., 1991, Georgia Basin Project: stratigraphy and structure of Gambier Group rocks in the Howe Sound-Mamquam River area, southwest Coast Belt: British Columbia: Geological Survey of Canada, Report of Activities, Paper, p. 49-58.

McFarland, C. R., 1983, Oil and gas exploration in Washington, 1900-1982: Washington Div. of Geology and Earth Resources, Olympia (USA).

McGarr, A., Simpson, D., Seeber, L., and Lee, W., 2002, Case histories of induced and triggered seismicity: International Geophysics Series, v. 81, no. A, p. 647-664.

Metz, B., Davidson, O., De Coninck, H., Loos, M., and Meyer, L., 2005, IPCC special report on carbon dioxide capture and storage, Cambridge: Cambridge University Press.

Miller, G. M., and Misch, P., 1963, Early Eocene angular unconformity at western front of northern Cascades, Whatcom County, Washington: AAPG Bulletin, v. 47, no. 1, p. 163-174.

Milne, W., Rogers, G., Riddihough, R., McMechan, G., and Hyndman, R., 1978, Seismicity of western Canada: Canadian Journal of Earth Sciences, v. 15, no. 7, p. 1170-1193.

Miri, R., and Hellevang, H., 2016, Salt precipitation during CO2 storage—A review: International Journal of Greenhouse Gas Control, v. 51, p. 136-147.

Molnar, S., Cassidy, J., Dosso, S., and Olsen, K., 3D Ground Motion in the Georgia Basin Region of SW British Columbia for Intra-slab Earthquake Scenarios, *in* Proceedings AGU Spring Meeting Abstracts2009, Volume 2009, p. S31A-05.

Monger, J., and Journeay, J., 1994, Basement geology and tectonic evolution of the Vancouver region: Geological Survey of Canada, Bulletin, v. 481, p. 3-25.

Monger, J., and Price, R., 2002, The Canadian Cordillera: geology and tectonic evolution: CSEG Recorder, v. 27, no. 2, p. 17-36.

Moore, J., Adams, M., Allis, R., Lutz, S., and Rauzi, S., 2005, Mineralogical and geochemical consequences of the long-term presence of CO2 in natural reservoirs: an example from the Springerville–St. Johns Field, Arizona, and New Mexico, USA: Chemical geology, v. 217, no. 3-4, p. 365-385.

Mosher, D. C., Cassidy, J. F., Lowe, C., Mi, Y., Hyndman, R. D., Rogers, G. C., and Fisher, M., 2000, Neotectonics in the Strait of Georgia: first tentative correlation of seismicity with shallow geological structure in southwestern British Columbia.

Mustard, P., 1991, Stratigraphy and sedimentology of the Georgia Basin, British Columbia and Washington State: Washington Geology, v. 19, p. 4.

Mustard, P. S., and Monger, J., 1994, The upper cretaceous Nanaimo group, Georgia basin: Geology and geological hazards of the Vancouver region, southwestern British Columbia. Edited by JWH Monger. Geological Survey of Canada, Bulletin, v. 481, p. 27-95.

Mustard, P. S., and Rouse, G. E., 1991, Sedimentary outliers of the eastern Georgia Basin margin, British Columbia: Current research, part A. Geological Survey of Canada, Paper, v. 91, p. 229-240.

Mustard, P. S., Rouse, G.E. and Monger, J. , 1994, Stratigraphy and evolution of Tertiary Georgia Basin and subjacent Upper Cretaceous sedimentary rocks, southwestern British Columbia and northwestern Washington State; in Geology and Geological Hazards of the Vancouver Region, Southwestern British Columbia: Geological Survey of Canada,, v. 481, p. 97-169.

Na, J., Xu, T., Yuan, Y., Feng, B., Tian, H., and Bao, X., 2015, An integrated study of fluid–rock interaction in a CO2-based enhanced geothermal system: A case study of Songliao Basin, China: Applied Geochemistry, v. 59, p. 166-177.

Nordbotten, J. M., Celia, M. A., and Bachu, S., 2005, Injection and storage of CO 2 in deep saline aquifers: analytical solution for CO 2 plume evolution during injection: Transport in Porous media, v. 58, p. 339-360.

Oldenburg, C. M., 2012, The risk of induced seismicity: Is cap-rock integrity on shaky ground?

Pachauri, R. K., Allen, M. R., Barros, V. R., Broome, J., Cramer, W., Christ, R., Church, J. A., Clarke, L., Dahe, Q., and Dasgupta, P., 2014, Climate change 2014: synthesis report. Contribution of Working Groups I, II and III to the fifth assessment report of the Intergovernmental Panel on Climate Change, Ipcc.

Pearce, J., La Croix, A., Brink, F., Hayes, P., and Underschultz, J., 2021, CO2 mineral trapping comparison in different regions: predicted geochemical reactivity of the Precipice Sandstone reservoir and overlying Evergreen Formation: Petroleum Geoscience, v. 27, no. 3.

Pearce, J., La Croix, A., Underschultz, J., and Golding, S., 2020, Long term reactivity of CO2 in a low salinity reservoir-seal complex: Applied Geochemistry, v. 114, p. 104529.

Piri, M., Prévost, J. H., and Fuller, R., Carbon dioxide sequestration in saline aquifers: evaporation, precipitation and compressibility effects, *in* Proceedings Fourth annual conference on carbon capture and sequestration DOE/NETL2005.

Portal, W. G. I., 2023.

Pruess, K., Xu, T., Apps, J., and Garcia, J., 2003, Numerical modeling of aquifer disposal of CO2: Spe Journal, v. 8, no. 01, p. 49-60.

Ringrose, P., 2020, How to store CO2 underground: Insights from early-mover CCS projects, Springer.

Rosenbauer, R. J., and Thomas, B., 2010, Carbon dioxide (CO2) sequestration in deep saline aquifers and formations: Chapter 3.

Rouse, G. E., Lesack, K. A., and White, J. M., 1990, Palynology of Cretaceous and Tertiary strata of Georgia Basin, southwestern British Columbia: Current Research, Part F, Geological Survey of Canada, Paper, p. 109-113.

Rutqvist, J., Birkholzer, J., Cappa, F., and Tsang, C.-F., 2007, Estimating maximum sustainable injection pressure during geological sequestration of CO2 using coupled fluid flow and geomechanical fault-slip analysis: Energy Conversion and Management, v. 48, no. 6, p. 1798-1807.

Shafeen, A., Croiset, E., Douglas, P., and Chatzis, I., 2004, CO2 sequestration in Ontario, Canada. Part I: storage evaluation of potential reservoirs: Energy Conversion and Management, v. 45, no. 17, p. 2645-2659.

Shi, J., and Durucan, S., 2005, CO2 storage in deep unminable coal seams: Oil & gas science and technology, v. 60, no. 3, p. 547-558.

Shukla, R., Ranjith, P., Haque, A., and Choi, X., 2010, A review of studies on CO2 sequestration and caprock integrity: Fuel, v. 89, no. 10, p. 2651-2664.

Spellman, F. R., 2014, Environmental impacts of renewable energy, CRC press.

Sproule, J. C. P. R. U. G. S. P. L. F. V., British Columbia., 1976, Underground Gas Storage Prospects Lower Fraser Valley, British Columbia.: Sproule Associates Ltd.

Spycher, N., and Pruess, K., 2005, CO2-H2O mixtures in the geological sequestration of CO2. II. Partitioning in chloride brines at 12–100 C and up to 600 bar: Geochimica et Cosmochimica Acta, v. 69, no. 13, p. 3309-3320.

Stephenson, M. H., Ringrose, P., Geiger, S., Bridden, M., and Schofield, D., 2019, Geoscience and decarbonization: current status and future directions: Petroleum Geoscience, v. 25, no. 4, p. 501-508.

Strategy, M. o. E. a. C. C., 2023, Distribution of Large BC Industry GHG Emissions, Tableau Public.

Survey, U. S. G., 2023, Earthquakes Map.

Todd, D. K., and Mays, L. W., 2004, Groundwater hydrology, John Wiley & Sons.

Underschultz, J., Boreham, C., Dance, T., Stalker, L., Freifeld, B., Kirste, D., and Ennis-King, J., 2011, CO2 storage in a depleted gas field: An overview of the CO2CRC Otway Project and initial results: International Journal of Greenhouse Gas Control, v. 5, no. 4, p. 922-932.

Van der Flier-Keller, E., and Dumais, S., 1988, INORGANIC MATTER CONTENT AND SPECIALIZED ELEMENT POTENTIAL OF THE NANAIMO AND COMOX COALFIELDS, VANCOUVER ISLAND*(92G7 F, K).

Wolhuter, A., Garnett, A., and Underschultz, J., 2019, Notional injection site identification report.

Worden, R. H., 2023, Value of core for reservoir and top-seal analysis for carbon capture and storage projects: Geological Society, London, Special Publications, v. 527, no. 1, p. SP527-2022-2038.

Xu, T., Apps, J. A., and Pruess, K., 2003, Reactive geochemical transport simulation to study mineral trapping for CO2 disposal in deep arenaceous formations: Journal of Geophysical Research: Solid Earth, v. 108, no. B2.

-, 2004, Numerical simulation of CO2 disposal by mineral trapping in deep aquifers: Applied geochemistry, v. 19, no. 6, p. 917-936.

Zeidouni, M., Pooladi-Darvish, M., and Keith, D., 2009, Analytical solution to evaluate salt precipitation during CO2 injection in saline aquifers: International Journal of Greenhouse Gas Control, v. 3, no. 5, p. 600-611.

Zelt, B., Ellis, R., Zelt, C., Hyndman, R., Lowe, C., Spence, G., and Fisher, M., 2001, Three-dimensional crustal velocity structure beneath the Strait of Georgia, British Columbia: Geophysical Journal International, v. 144, no. 3, p. 695-712.

Zendehboudi, S., Khan, A., Carlisle, S., and Leonenko, Y., 2011, Ex situ dissolution of CO2: a new engineering methodology based on mass-transfer perspective for enhancement of CO2 sequestration: Energy & fuels, v. 25, no. 7, p. 3323-3333.

Zendehboudi, S., Leonenko, Y., Shafiei, A., Soltani, M., and Chatzis, I., 2012, Modeling of CO2 droplets shrinkage in ex situ dissolution approach with application to geological sequestration: Analytical solutions and feasibility study: Chemical engineering journal, v. 197, p. 448-458.

Zhai, L. a. G., S.E, 2015, Petrographic Study of the Nanaimo Group from OW-11-01-Nanaimo Obs Well 390, *in* Canada, G. S. o., ed., p. 74.

Zhang, D., and Song, J., 2014, Mechanisms for geological carbon sequestration: Procedia IUTAm, v. 10, p. 319-327.

Zirrahi, M., Hassanzadeh, H., and Abedi, J., 2013, The laboratory testing and scale-up of a downhole device for CO2 dissolution acceleration: International Journal of Greenhouse Gas Control, v. 16, p. 41-49.

Zoback, M. D., and Gorelick, S. M., 2012, Earthquake triggering and large-scale geologic storage of carbon dioxide: Proceedings of the National Academy of Sciences, v. 109, no. 26, p. 10164-10168.

Zweigel, P., Arts, R., Lothe, A. E., and Lindeberg, E. B., 2004, Reservoir geology of the Utsira Formation at the first industrial-scale underground CO2 storage site (Sleipner area, North Sea): Geological Society, London, Special Publications, v. 233, no. 1, p. 165-180.